This is a preprint, the final version is subject to change, of the American Mineralogist (MSA)
Cite as Authors (Year) Title. American Mineralogist, in press.
DOI: https://doi.org/10.2138/am-2018-6567

REVISION 2: TRIOCTAHEDRAL MICAS FROM THE CATALÃO CARBONATITE INTRUSIONS (ALTO PARANAÍBA, BRAZIL): CRYSTAL CHEMISTRY AND PETROGENETIC IMPLICATIONS

Vincenza Guarino[1]* and Maria Franca Brigatti[2]

[1]Dipartimento di Scienze della Terra, dell'Ambiente e delle Risorse, Università di Napoli Federico II, Complesso Universitario Monte Sant'Angelo, Ed. L, Via Cintia 26, 80126 Naples, Italy

[2]Dipartimento di Scienze Chimiche e Geologiche, Università degli Studi di Modena e Reggio Emilia, via G. Campi 103, I-41125 Modena, Italy

*Corresponding Author: vincenza.guarino@unina.it

RUNNING TITLE: Trioctahedral micas from the Catalão carbonatite intrusions

This is a preprint, the final version is subject to change, of the American Mineralogist (MSA)
Cite as Authors (Year) Title. American Mineralogist, in press.
DOI: https://doi.org/10.2138/am-2018-6567

ABSTRACT

The Catalão II and Catalão I carbonatite complexes are Cretaceous intrusions in the north-western part of the Alto Paranaíba Igneous Province, central Brazil, and contain a variety of trioctahedral micas ~~that we have studied~~. Drill-hole sampling and mineralogical and geochemical data suggest the existence of different types of cumulate rocks as carbonatites (calcio- and ferrocarbonatites in Catalão II; magnesiocarbonatites in Catalão I), magnetitites, apatitites and phlogopitites. In Catalão II complex the presence of ultramafic lamprophyres (phlogopite-picrites) and fenites (syenites and clinopyroxenites) are identified. Phlogopite, Fe^{3+}-rich phlogopite and tetraferriphlogopite are ubiquitous, with marked and variable pleochroism. In the Catalão II, micas from magnetitites, apatitites and calciocarbonatites are close in composition to the tetraferriphlogopite end member. The $Mg/(Mg+{}^{[VI]}Fe_{tot})$ average value is 0.959 for micas from magnetitites, 0.878 for micas from apatitites, and 0.875 for micas from calciocarbonatites, suggesting an enrichment of octahedral iron in crystals from calciocarbonatites. The trioctahedral micas from the fenites are intermediate in composition between phlogopite and tetraferriphlogopite, with $0.227 \leq {}^{[IV]}Fe \leq 0.291$ apfu. Micas of phlogopitites, ferrocarbonatites and phlogopite-picrites show a significant variation in $^{[IV]}Fe$, $^{[IV]}Al$, $^{[VI]}Mg$ and $^{[VI]}Fe$ contents, suggesting the existence of different mica populations. In the Catalão I magnetitites micas show a quite ~~constant Mg~~ but marked differences in $^{[IV]}Fe^{3+}$ and $^{[IV]}Al$ content, so there are $^{[IV]}Fe^{3+}$-bearing phlogopite and tetraferriphlogopite. The micas from Catalão I apatitites have variable $^{[IV]}Fe^{3+}$, $^{[IV]}Al$ and Mg contents and are mainly tetraferriphlogopite with a minor phlogopite population. Trioctahedral micas from Catalão I magnesiocarbonatites contain crystals close to tetraferriphlogopite with $^{[IV]}Fe^{3+}$ and a limited variation in Mg content. In these complexes, heterovalent octahedral substitutions are mainly related to Ti^{4+} and, only in a few samples, to Fe^{3+}. The primary mechanism regulating Ti uptake into the mica structure is the Ti-oxy $[{}^{[VI]}Ti^{4+}{}^{[VI]}(Mg, Fe)^{2+}_{-1}(OH)^{-}_{-2}O^{2-}_{2}]$ substitution. Crystal structural analysis shows that all mica crystals are 1*M* polytypes with the expected space group *C*2/*m*. The nearly equal size and

mean electron count between M1 and M2 octahedral sites suggest disorder of octahedral cations between these two sites. The low Al and the high Fe^{3+} content in the tetrahedral site of these micas, as well as the high $(OH)^-$ content, reflects the general enrichment in FeO and H_2O and the peralkaline nature of magma from which Catalão I and Catalão II micas crystallized. Micas strongly enriched in Fe^{3+} and poor in Ti and Al, are used, for the first time, as indicators of crystallization temperature using published geothermometers. Temperatures range between ~ 800 and 558 °C for the Catalão II cumulate rocks, in high oxygen fugacity conditions, mainly over the HM condition. In contrast, the variability in temperature (703-631 °C and 1050-952 °C) for Catalão II phlogopite-picrites is consistent with mica crystallization in an HM-NiNiO environment. The ~~obtained~~, temperatures for Catalão I cumulate rocks (742-542 °C for magnesiocarbonatites, 923-540 °C for magnetitites, and 679-550 °C for apatitites) are quite similar with those of Catalão II rocks, but they show generally ~~a high~~, oxygen fugacity conditions (over HM condition).

Keywords: phlogopite, tetraferriphlogopite, carbonatites, Catalão, Alto Paranaíba Igneous Province, Brazil

INTRODUCTION

Several studies related layer topology of trioctahedral micas to crystallization conditions (Brigatti et al. 1996, 2000a, 2000b, 2001; Laurora et al. 2007; Lacalamita et al. 2011; Schingaro et al. 2011; Scordari et al. 2013 and references therein). Determining the changes in layer topology of trioctahedral micas under changing crystallization conditions is not simple because most igneous micas have a complex geologic history (Brigatti et al. 1996; Scordari et al. 2013; Schingaro et al. 2014) that may consist of multi-step processes, under non-equilibrium conditions. Thus, complex crystal chemistry could reflect a complex genetic history. Trioctahedral micas show different substitution mechanisms, which affect

different structural sites, as charge balance can be achieved either within one site only or by involving several sites. The geometrical variation of the mica layer as a result of a given compositional substitution is thus not always linear and can be complex (Brigatti et al. 2003, 2016).

Phlogopite [$KMg_3AlSi_3O_{10}(F,OH)_2$] and tetraferriphlogopite [$KMg_3Fe^{3+}Si_3O_{10}(OH)_2$] are common mafic phases in alkaline-carbonatite complexes; their crystal chemical features are thought to be related to the composition of the magma from which they crystallized (Krivdik et al. 1982; Bagdasarov et al. 1985; Heathcote and McCormick 1989; Gibson et al. 1995, 2006; Brigatti et al. 1996; Kamenetsky et al. 2009), as well as to the pressure (P) and temperature (T) of crystallization (Kamenetsky et al. 2009; Naemura et al. 2009). A crystal chemical study of micas from Tapira carbonatites (Brigatti et al. 1996) indicated that they crystallized in two different stages of the magma evolution, both characterized by low-P and high- f_{O_2} conditions, i.e., from alkaline-silicate magmas (in this case mica phlogopite with moderate to low substitution of $^{[IV]}Fe^{3+}$ for $^{[IV]}Si$) or from silicate-carbonatite magmas (in this case strong $^{[IV]}Fe^{3+}$ for $^{[IV]}Si$ substitution occurs in the presence of very high f_{O_2}, a_{H_2O}, and CO_2).

This study provides a detailed crystal-chemical characterization of trioctahedral micas, belonging to the phlogopite – annite and to the tetraferriphlogopite – tetraferriannite joins, from the Catalão intrusions in Brazil. The results highlight the importance of understanding substitution mechanisms when applying them to strongly Fe^{3+}-enriched phlogopite crystals for the purpose of constraining crystallization conditions, principally in terms of T and oxygen fugacity, during rock formation.

GEOLOGICAL SETTING

The Catalão I and Catalão II complexes are located in the Alto Paranaíba Igneous Province (Figure 1) in the south-eastern part of Goiás and the western part of Minas Gerais. This province is one of the largest ultrapotassic/kamafugitic provinces of the world, and extends over ~20,000 km^2 between the

São Francisco Craton and the north-eastern border of the Paraná Basin (south-eastern Brazil) (Figure 1 *inset*). It was formed by emplacement of strongly alkaline and carbonatite rocks (mostly kamafugites, kimberlites, lamprophyres and carbonatites) found as lava flows, pyroclastic successions and hypabyssal intrusions (Gibson et al. 1995; Brod et al. 2000, 2001; Araújo et al. 2001; Read et al. 2004; Gomes and Comin-Chiaramonti 2005; Melluso et al. 2008; Guarino et al. 2013, 2017).

The Catalão I and Catalão II complexes intruded the Araxá Group (quartzites, schists, and phyllites) of the Late Proterozoic Brasília Belt (Almeida et al. 2000). These complexes are located along a NW-SE lineament that controlled the emplacement of Cretaceous alkaline rocks of the Alto Paranaíba Igneous Province (Biondi 2005). The Catalão I complex (18°08′ S, 47°50′ W; Cordeiro et al. 2011 and references therein) has a circular dome-shape 27 km^2 in size, with a diameter of 5.5-6.0 km, with the carbonatites at the center, in veins and dykes, which cut cross the other alkaline mafic rocks. Mantovani et al. (2016) estimated the shape and volume for the carbonatite body of Catalão I complex (about 1.99 km^3) utilizing gravity and magnetic data. The Catalão II complex (18°02′ S, 47°52′ W, 5 x 2.7 km; Guarino et al. 2017 and references therein) consists of two pipes, with a total ~~circular~~ shape of 14 km^2, that are about 2 km apart; it constructed through the sequential emplacement of dykes, veins and alkaline igneous bodies emplaced in a complex pattern (Machado 1991; Rocha et al. 2001). The Catalão II complex is known for the alteration of magmatic pyrochlore into secondary phases during supergene alteration processes in the alteration cover, and related mineralization (Rocha et al. 2001; Guimarães and Weiss 2013). The Catalão I rocks have been obtained through three boreholes F72, 3E19N and 49E33N while Catalão II rocks ~~through~~ two drill cores, penetrating the ~50 m-thick lateritic soil (Rocha et al. 2001), C3B2(A) and C3B1(B) boreholes in the south and north pipes, respectively. Details on sampled rocks and their modal mineralogy are given in Table 1, where samples are ordered following their drill-hole depth (cf. Guarino et al. 2017).

PETROGRAPHY

Modal and compositional data were used to classify the Catalão I and II rocks (Table 1; Guarino et al. 2017). The Catalão I complex consists of lamprophyric dykes (Gomes and Comin-Chiaramonti 2005), phoscorites (Cordeiro et al. 2011), apatitites, magnetitites and magnesiocarbonatites with cumulate texture (Guarino et al. 2017 and references therein). The Catalão II complex is characterized by the presence of ultramafic lamprophyres (as phlogopite-picrites, Guarino et al. 2013), apatitites, magnetitites, calciocarbonatites, ferrocarbonatites, phlogopitites and fenitized rocks or fenites (syenites and amphibole clinopyroxenites). The identified lithologies show inequigranular holocrystalline, cumulate texture, with the exception of the phlogopite-picrites that have a porphyritic and pseudo-fluidal texture and clinopyroxenites with banded ~~texture.~~

Catalão I rocks. Magnesiocarbonatites ~~are made~~ of cryptocrystalline carbonate or ~~by~~ medium- to coarse-grained carbonate (dolomite and/or magnesite) crystals, associated with minor amounts of carbonates, phlogopite, apatite and zoned pyrochlore crystals. Apatitites have apatite as predominant mineral, with ~~presence of~~ magnetite, phlogopite, carbonate and pyrochlore. Magnetitites are characterized by magnetite and subordinate phlogopite, apatite and pyrochlore.

Catalão II rocks. The phlogopite-picrites show a porphyritic and pseudo-fluidal texture with olivine and phlogopite phenocrysts in a groundmass rich in phlogopite laths with olivine, spinel, apatite, perovskite, calcite and rare garnet and rutile. The calciocarbonatites and ferrocarbonatites are characterized by medium- to coarse-grained anhedral carbonates and minor amounts of macro- and microcrystals of zoned phlogopite (slightly orange in the core and dark orange in the rims), apatite, magnetite, pyrochlore, carbonates, rutile, rare clinopyroxene and amphibole. The magnetitites are characterized by medium-to-coarse-grained magnetite associated with subordinate phlogopite, apatite, pyrochlore and carbonates. The apatitites are medium- to coarse-grained rocks and consist of apatite and phlogopite, with minor opaque minerals, carbonates and pyrochlore. Phlogopitites have phlogopite as

the dominant phase, minor magnetite, pyrochlore, apatite and very rare carbonates. The syenite C2A6 is dominated by alkali feldspar, with minor Na-rich clinopyroxene, phlogopite, amphibole and apatite. The clinopyroxenite C2A26 has a banded structure, with Na-rich clinopyroxene and amphibole bands alternate with minor phlogopite bands. Apatite and carbonate are accessory phases. Syenite and amphibole clinopyroxenite are fenites, i.e., the products of interaction between the host rocks and Na- and K-rich fluids, likely derived from the carbonatite intrusion (Le Bas 2008; Guarino et al. 2012). All phlogopite crystals, both in Catalão I and II rocks, show marked and variable pleochroism, from light-to-dark orange into the cores of crystals or in single crystals, and from orange to dark red, observable along the rims and in single crystals (**Supplemental[1] Figures** 1 and 2).

EXPERIMENTAL METHODS

Thin sections of the Catalão I and Catalão II rocks were observed using polarized light microscopy, with a Leitz Laborlux 12 POL microscope, to identify the mineral phases. Modal analysis, based on 3000 points, was carried out with Leica Q Win software equipped with a Leica DFC280 camera (Table 1).

Mineral composition and calculation of stoichiometric formula. Compositional analyses were performed, both on polished thin sections (Table 2) and on the same crystals used for structure refinement (Table 3), on a Cameca SX50 ~~electron microprobe~~. The following operating conditions were used: accelerating voltage 20 kV, sample current 20 nA, and defocused beam diameter 4 μm. The F content was determined from the method reported by Foley (1989). No evidence of F volatilization was observed after 40 s counting time, as reported in Signorelli et al. (1999). Individual point analyses for each homogeneous crystal were averaged, and rim-core compositional variation was observed to be within 3% of the estimated standard error for each element (3% relative), indicating a high degree of compositional homogeneity. Thin-section samples occasionally showed the coexistence of two mica

populations (Table 2), the different populations are identified by labels (a) and (b), respectively. When different populations are not present, averaged data refer to mica samples belonging to the same population. The FeO content of crystals used for structure refinement were determined using the procedure of Meyrowitz (1970) with an estimated standard deviation $\sigma < 4\%$. The $(OH)^-$ content was derived from thermogravimetric analysis in He gas flow using a Seiko SSC 5200 thermal analyzer (heating rate 10 °C/min and gas flow rate 100 µl/min), equipped with a mass spectrometer (GeneSys ESS, Quadstar 422). Stoichiometric formulae of micas analyzed on polished thin sections were calculated based on a -22 charge (Table 2). Hydroxyl content was estimated by filling the anionic site (i.e., OH+F=2). Similarly, the Fe^{2+}/Fe^{3+} ratio was derived by assuming full occupancy of the tetrahedral site (i.e., $Si^{4+}+Al^{3+}+Fe^{3+} = 4$) by using the total tetrahedral electron density, and by approaching, as closely as possible, the octahedral and interlayer theoretical occupancies. The stoichiometric formulae for the crystals used for structure refinement were calculated by an iterative approach (Table 3). As a first step, the charges of cations in tetrahedral, octahedral and interlayer sites were set equal to 22. The composition of the anion site, populated by $(OH)^-$, F^- and O^{2-}, was a result of this step. Given $X = 2- [(OH)^-+F^-)]$, the stoichiometric formula was calculated assuming 22+X positive charges for tetrahedral, interlayer and octahedral sites, which leads to an assessment of anion composition and therefore to a value for X. The iterative procedure was used until the difference in the X value from each step, was $< 10^{-7}$.

Additional compositional data. Compositional data for micas from the Catalão II and Catalão I rocks shown in tetrahedral plots (see Supplemental[1] Table 1) were determined on polished thin sections with an energy dispersive spectrometer (EDS) at Dipartimento di Scienze della Terra, dell'Ambiente e delle Risorse (Di.S.T.A.R.), University of Napoli Federico II (a JEOL JSM-5310 microscope and an Oxford Instruments Microanalysis Unit, equipped with an INCA X-act detector). Full analytical details, including all utilized standards, are reported in Melluso et al. (2014, 2017) and Guarino et al. (2017).

X-ray-diffraction. Each single crystal was mounted on a Bruker X8-Apex automated four-circle diffractometer with Kappa geometry, equipped with a fine-focus Mo ceramic X-ray tube (λ = 0.7107 Å) and APEX 4K CCD detector. Data collection used the APEX2 software. Preliminary unit-cell parameters and an orientation matrix were obtained from three sets of frames and were refined during the integration process of intensity data. Diffraction data were collected with ω scans at specific φ settings (φ–ω scan). Data were processed using SAINT Plus (Bruker 2003). The SADABS package (Sheldrick 1996) was used to perform a semi-empirical absorption correction. Space group determination and data merging were performed using XPREP (Sheldrick 1997). Crystal structures were refined using the SHELX-97 package of programs (Sheldrick 1997). Information related to X-ray data collection and refinements, as well as the unit-cell parameters of the measured micas, are available from the CIF file. Structure refinements were performed following the assumptions previously adopted by Laurora et al. (2007) for ferroan phlogopite. Atomic-position parameters of the 1*M* mica polytype from Laurora et al. (2007) were assumed as initial values. Appropriate neutral scattering factors were used for both cation and anion positions. Tetrahedral occupancy was refined assuming Si and Al^{3+}, Si and Fe^{3+} and a combination of Si, Al^{3+} and Fe^{3+}. Octahedral occupancy was refined assuming Mg, Fe^{2+}, Fe^{3+} and Ti occupancy. In the final cycles, anisotropic displacement parameters were refined for all atoms. The occupancy at each tetrahedral and octahedral site was verified against measured interatomic distances, mean atomic number, and chemical formula by using an iterative procedure minimizing discrepancies with measured mean electron count, interatomic distances (experimental vs. calculated from Shannon radii and assumed chemical population of the site; Shannon 1976). Table 3 reports octahedral and interlayer mean electron count (m.e.c.) from crystal structure refinements and, for comparison, from electron microprobe measurements. Final refinements yielded the agreement factor values (*R*), the atom coordinates and equivalent isotropic and anisotropic displacement factors are available from the CIF file. The final calculated difference electron density maps did not reveal

207 significant excess electron density above background. Table 4 lists relevant cation-anion bond lengths
208 and selected geometrical parameters obtained from structure refinements.
209
210 **PHLOGOPITE COMPOSITIONS**
211 Representative compositions of phlogopite crystals are reported in Tables 2 and 3. The number of
212 atoms per formula unit was calculated following two normalization procedures as reported in the
213 Experimental Methods section. For this reason, compositional ranges reported in this section refer to
214 Table 2 only.
215 In Catalão I and Catalão II micas, the Si and Al contents in tetrahedral sites are always < 4 apfu (Figure
216 2a), suggesting that these micas include $^{[IV]}Fe^{3+}$-rich phlogopite and tetraferriphlogopite (Bailey 1984)
217 because variable amounts of Fe^{3+} were required to complete the tetrahedral site occupancy. The
218 tetrahedral Fe^{3+} and total Al contents are negatively correlated, and the analytical points plot close to
219 the line $^{[IV]}Fe/Al = 1/1$ (Figure 2b, Table 2). Above $^{[IV]}Fe \cong 0.9$ apfu the $^{[IV]}Fe$ increases, but Al remains
220 constant. Thus, the tetraferriphlogopite end-member shows a lower amount of Si substitution with
221 respect to phlogopite. When plotted in the classification diagram *mgli* vs. *feal* [i.e., *mgli* = $^{[VI]}$(Mg - Li);
222 *feal* = $^{[VI]}(Fe_{total} + Mn + Ti - Al)$, Tischendorf et al. 2004], the Catalão I and Catalão II micas present
223 octahedral compositions intermediate between phlogopite and annite (Figure 3), but most of the
224 samples plot in the phlogopite sector. A few crystals from Catalão II rocks (C2B24 ferrocarbonatite,
225 C2A10 and C2A18 phlogopite-picrites) plot in the annite sector.
226 Micas from the Catalão I complex are richer in Mg (2.736-2.960 apfu) when compared with micas
227 from the Catalão II complex (Mg 1.125-2.806 apfu; Table 2). Lower Mg content is compensated by
228 higher $^{[VI]}Fe_{tot}$ content in samples from Catalão II micas, reaching an average value of 0.463 apfu,
229 which is statistically greater than the values observed in Catalão I samples (i.e., average value of 0.084
230 apfu). Ti content is also greater in samples from Catalão II when compared with samples from Catalão

I, with average values of 0.084 and 0.006 apfu, respectively. Titanium is inversely correlated with Mg (Figure 4a) for all samples but not for micas in Catalão II phlogopite-picrites, which are also characterized by highest Ti (0.170-0.268 apfu) content. On the opposite side, tetraferriphlogopite crystals from Catalão I are Mg rich and almost completely Ti free.

Catalão trioctahedral micas are characterized by high compositional variability among different rock types (see Table 2). In fact, the trioctahedral micas from Catalão II magnetitites, apatitites and calciocarbonatites are tetraferriphlogopite ($^{[IV]}Al \leq 0.187$ apfu). Magnesium is always the main octahedral cation, with an $Mg/(Mg+ {}^{[VI]}Fe_{tot})$ average value of 0.959 for micas from magnetitites, 0.878 for micas from apatitites and 0.875 for micas from calciocarbonatites. Trioctahedral micas from Catalão II fenites (syenite and clinopyroxenite) are intermediate in composition between phlogopite and tetraferriphlogopite. Micas from Catalão II phlogopitites, ferrocarbonatites and phlogopite-picrites show a high variation in $^{[IV]}Fe$ (0.311-0.979 apfu in phlogopitite, 0.497-0.996 apfu in ferrocarbonatites, 0.097-0.924 apfu in phlogopite-picrites), $^{[IV]}Al$ (0.009-0.727 apfu in phlogopitite, 0.007-0.516 apfu in ferrocarbonatites, 0.127-1.051 apfu in phlogopite-picrites) and $^{[VI]}Mg$ (2.137-2.572 apfu in phlogopitite, 1.159-2.384 apfu in ferrocarbonatites, 1.125-2.604 apfu in phlogopite-picrites) contents, suggesting the presence of different mica populations.

Trioctahedral micas from Catalão I magnetitites show marked differences in $^{[IV]}Fe^{3+}$ (0.124-1.002 apfu) and $^{[IV]}Al$ (0-0.925 apfu) content, unlike Mg (2.873-2.960 apfu) that remains quite constant, suggesting coexistence of $^{[IV]}Fe^{3+}$-bearing phlogopite and tetraferriphlogopite. Trioctahedral micas from Catalão I apatitites are mainly tetraferriphlogopite with a minor phlogopite population and show variable $^{[IV]}Fe^{3+}$ (0.069-0.931 apfu), $^{[IV]}Al$ (0.003-1.049 apfu) and Mg (2.773-2.943 apfu) contents, with Ti content close to zero. Trioctahedral micas from Catalão I magnesiocarbonatites contain crystals close to tetraferriphlogopite with $^{[IV]}Fe^{3+}$ (0.617-0.929 apfu) and a limited variation in Mg (2.736-2.870 apfu) content.

CRYSTAL STRUCTURE AND CRYSTAL CHEMISTRY

The trioctahedral micas belong to space group *C*2/*m* and are 1*M* polytypes (see CIF file). The main exchange mechanisms that control the layer topology are both homovalent substitutions $^{[IV]}Fe^{3+}\ ^{[IV]}Al^{3+}_{-1}$ and $^{[VI]}Fe^{2+}\ ^{[VI]}Mg^{2+}_{-1}$ and heterovalent substitutions, such as $^{[VI]}Ti^{4+}\ ^{[VI]}Mg^{2+}_{-1}(OH)^{-}_{-2}$, and $^{[VI]}Fe^{3+}O^{2-}\ ^{[VI]}Fe^{2+}_{-1}(OH)^{-}_{-1}$. Changes in geometrical parameters can thus be related to compositional changes in both tetrahedral and octahedral sites. Tetrahedral parameters such as tetrahedral volume, flattening angle τ, and Δz reflect $^{[IV]}Fe^{3+}$ content because $^{[IV]}Fe^{3+}$ substitution produces an increase in tetrahedral volume and a flattened tetrahedron in tetraferriphlogopite with respect to phlogopite. The increase of the tetrahedral volume, associated with an increase in tetrahedral basal dimensions and in the area defined by tetrahedral basal oxygen atoms ($^{[IV]}\langle$O-O$\rangle$; Table 4), is also reflected in the octahedral site, showing an increase in unshared ⟨O3-O3⟩ edges with increasing $^{[IV]}Fe^{3+}$ content (Figure 4b). The deviation of samples of Catalão II ferrocarbonatite C2B24 and fenite C2A26 from the above-mentioned trends can be associated with high $^{[VI]}Fe^{2+}$ content that produces an increase in ⟨O3-O3⟩ edges. These two samples ~~are~~ also those ~~showing~~ a lower tetrahedral rotation α which is a measure of tetrahedral to octahedral dimensional misfit (Brigatti et al. 2003). In most of the other samples in our dataset, α increases with $^{[IV]}Fe^{3+}$ content, because the increase imparted on ⟨O3-O3⟩ is insufficient to fully compensate for the increase in tetrahedral basal dimensions. The $^{[IV]}Fe^{3+}\ ^{[IV]}Al^{3+}_{-1}$ substitution, which defines the phlogopite to tetraferriphlogopite join, increases the dimensions of the tetrahedral site and requires the extension of the octahedral triads.

Fe^{2+} for Mg^{2+} octahedral substitution induces an increase in ⟨M1-O⟩ mean bond distance, as is common in trioctahedral micas (Brigatti and Guggenheim 2002), and in the area of the hexagon defined by

277 tetrahedral basal oxygen atoms (Figure 4c). So, the tetrahedral basal oxygen atoms, unlike what is
278 commonly observed in trioctahedral micas, is not related to α in all the mica samples ~~under study~~.
279 Most trioctahedral micas of both Catalão complexes (Table 4) show a difference (Δ⟨M-O⟩) between
280 ⟨M1-O⟩ and ⟨M2-O⟩ mean bond distances less than 0.006 Å (thus $\Delta\langle M\text{-}O\rangle \leq 3\sigma$, where σ is the
281 estimated standard deviation on the mean value). Thus, the nearly equal size and mean electron count
282 between M1 and M2 suggest disorder between octahedral cations. Only a few crystals from Catalão II
283 (C2A26 fenite, C2B19 calciocarbonatite and C2B24 ferrocarbonatite) show ⟨M1-O⟩ mean bond
284 distance greater than ⟨M2-O⟩ (Δ⟨M-O⟩ C2A26 = 0.009 Å; Δ⟨M-O⟩ C2B19 = 0.008 Å) and mean
285 electron count higher in M1 than in M2. Both these features suggest a preferential location of higher
286 atomic number and larger cations in the M1 site.
287
288 **IMPLICATIONS**
289 Phlogopite, tetraferriphlogopite and $^{[IV]}Fe^{3+}$-rich phlogopite are ubiquitous in Catalão rocks. The
290 complex mineralogical assemblages linked to the cumulate texture of the Catalão II host rocks
291 (calciocarbonatites, ferrocarbonatites, apatitites, magnetitites, and phlogopitites) make the establishment
292 of crystallization relationships between minerals extremely difficult. Phlogopite crystallizes together
293 with apatite (e.g., phlogopite encloses apatite or *vice-versa*), whereas magnetite probably began to
294 crystallize slightly before and even contemporaneously with phlogopite; carbonates are the last to
295 crystallize. Cumulate rocks and liquid phase compositions differ because rock formation occurred
296 through extensive accumulation processes caused by differential settling of the heavy phases (magnetite,
297 apatite, pyrochlore and sulfides), and their compositions are related to the different modal amounts of
298 minerals (Guarino et al. 2017). A ~~quite~~ similar process was defined for Catalão I cumulate rocks. ~~The~~
299 ~~different~~ settling, in addition to being visible in rock texture, is again ~~observable~~ ~~through the~~
300 ~~comparison,~~ for example, between mica compositions (and also with carbonates and opaque minerals)

and their Catalão II host related rocks (Supplemental[1] Figure 3). The behavior of micas analyzed in the phlogopite-picrites (Supplemental[1] Figure 3) is different, because the phlogopite-picrites in Catalão II can be interpreted as a result of a low degree partial melting (f =0.5-2%) of a mantle source consisting of a carbonated lherzolite with phlogopite-rich veins, strongly enriched in incompatible elements (Guarino et al. 2013 and references therein).

Tetrahedral Fe^{3+}, Al deficiency and Ti significance in the Catalão micas

The noteworthy compositional features of Catalão II micas are the high $^{[IV]}Fe^{3+}$ and low tetrahedral Al content, together with enrichment in $(OH)^-$. Tetrahedral Fe^{3+} variation is related to drill-core depth of Catalão II rocks (Table 5), although this variation is not fully representative of crystallization depth but rather of the depth of emplacement. Catalão II phlogopite crystals from calciocarbonatites show high $^{[IV]}Fe^{3+}$ concentrations and low $^{[IV]}Fe^{3+}$ variation ($0.880 \leq {}^{[IV]}Fe^{3+} \leq 0.985$ apfu) over a range of depths, likely due to the high oxygen fugacity of Catalão II magma from which they crystallized (Table 5). Similar values of $^{[IV]}Fe^{3+}$ can be observed in Catalão II apatitites and magnetitites, suggesting similar fugacity. These micas are also low in $^{[IV]}Al$ (≤ 0.3 apfu). The low $^{[IV]}Al$ content and the high $^{[IV]}Fe^{3+}$, together with high $(OH)^-$ contents, reflect the general enrichment in FeO and H_2O (as the predominant volatile) and the peralkaline nature of the magma from which Catalão II micas crystallized. The variability in $^{[IV]}Fe^{3+}$ concentration in the Catalão II ferrocarbonatites (0.497-0.996 apfu; Table 5) is associated with micas analyzed in two different samples. The C2B18 sample ($^{[IV]}Fe^{3+} = 0.996$ apfu) show values similar to those for the calciocarbonatites, thus suggesting similar crystallization conditions described above. Sample C2B24 shows a lower $^{[IV]}Fe^{3+}$ concentration (0.497 apfu) with respect to other studied micas from carbonatites, possibly suggesting that this carbonatite could be the result of a late-stage *carbothermal* residual magma (Mitchell 2005; Guarino et al. 2017).

Variable $^{[IV]}Fe^{3+}$ concentrations in Catalão I phlogopite crystals from magnesiocarbonatites ($0.617 \leq {}^{[IV]}Fe^{3+} \leq 0.929$ apfu), magnetitites ($0.124 \leq {}^{[IV]}Fe^{3+} \leq 1.002$ apfu) and apatitites ($0.069 \leq {}^{[IV]}Fe^{3+} \leq 0.931$ apfu) could be related to magmatic and weathering processes, as testified by the wide variation in their oxygen isotopes [$\delta^{18}O_{(V\text{-}SMOW)} = 6.13\text{-}10.75‰$] analyzed in different minerals (Guarino et al. 2017 and references therein).

Different hypotheses can be formulated to account for the Al deficiency in the tetrahedral site of micas: i) in lamproites and orangeites, Al deficiency can depend on the peralkalinity of the magma (Mitchell and Bergman 1991; Mitchell 1995); ii) several authors suggested that low Al concentration in the liquid and/or high $f(O_2)$ control the formation of tetraferriphlogopite (e.g., Arima and Edgar 1981; Heathcote and McCormick 1989; Brigatti et al. 1996); iii) tetraferriphlogopite crystallization in a carbonatite-bearing alkaline-ultrabasic complex can be attributed to the occurrence of oxidizing conditions during the late stages of carbonatite formation (Krasnova 2001) or iv) Gibson et al. (1995, 2006) that the Al-poor composition of most of the trioctahedral micas from the mantle can be attributed to the local post-emplacement crystallization environment rather than to the composition of the parent magma. The slightly higher Ti concentrations in Catalão I than in Catalão II micas (Figure 4a) may indicate that the Ti concentration in trioctahedral micas cannot be related only to coexisting mineral assemblages, but also to the physicochemical conditions prevailing during crystallization [i.e., T and $f(O_2)$ increase, P decrease; Greenwood 1998]. In spite of the low Ti content of the trioctahedral micas from Catalão I, there was moderate TiO_2 availability in the liquid, as testified by the presence of Ti-bearing phases (i.e., Ti-rich magnetite and ilmenite) in Catalão I magnetitites (Guarino et al. 2017). Thus, the variation in Ti content in micas can be attributed to both the mineral assemblage, including the presence of competing phases, e.g., magnetite or pyrochlore that may include the Ti in their chemical formula, to the nature of the magma and probably to the conditions of $f(O_2)$, $a(H_2O)$ and $f(CO_2)$ during the late stages of magmatic evolution.

348

349 **Chemical behavior of phlogopite in alkaline complexes (Brazil)**

350 Mica samples from Catalão I and Catalão II rocks are characterized by higher tetrahedral charge when
351 compared with mica crystals from Tapira rocks, defining a linear correlation showing a concomitant
352 octahedral charge increase with decreasing tetrahedral charge (Figure 4d). Micas from both Catalão
353 complexes are also characterized by a narrower compositional range when compared with micas from
354 Tapira, with compositions closer to the tetraferriphlogopite end-member. This feature suggests less
355 variability in intensive parameters (e.g., T and P) in force during crystallization. Deviation from the
356 above mentioned linear trend is in the micas analyzed in the Alto Paranaíba kamafugites, where
357 octahedral charge increases due to high site occupancy by Ti. This increase in octahedral charge is no
358 longer fully compensated by a decrease in tetrahedral charge (Figure 4d).
359 The increase in Ti content is associated with a decrease in $(OH)^-$ content and in A-O4 distance, thus
360 suggesting Ti-oxy substitution. This substitution is significantly more common in micas from Alto
361 Paranaíba kamafugites ~~rather~~ than in micas from Catalão and Tapira complexes (Figures 5a and 5b). If
362 Ti-oxy substitution is present in Catalão and Tapira rocks, it is not as significant as in Alto Paranaíba
363 kamafugite samples. This observation is consistent with different crystallization conditions in the Alto
364 Paranaíba kamafugites than in Catalão and Tapira rocks. This difference is due to the crystallization of
365 Ti-bearing minerals, such as perovskite/opaque minerals that are widely present in the Alto Paranaíba
366 rocks (kimberlites, kamafugites and phlogopite-picrites; Guarino et al. 2013). These different crystal
367 chemical mechanisms are also reflected in unit-cell parameter variation. In all considered samples, the *c*
368 parameter increases with the *a* and *b* parameters, they follow two different trends depending on the
369 amount and nature of the Ti substitution. With similar *a* and *b* parameters to those for samples from
370 Tapira, the Alto Paranaíba samples show lower *c* parameter values and smaller cell volumes. Samples
371 from the Catalão complexes are characterized by larger unit-cell parameters (Figure 6).

Through the tetraplot diagram (Cucciniello 2016), it is possible to correlate all tetrahedral cations with Mg as the main octahedral cation. These diagrams compare micas analyzed in the main alkaline and alkaline-carbonatite complexes identified in southern Brazil, including Catalão II, Catalão I, Tapira, Salitre and Araxá in the Alto Paranaíba Igneous Province, and Ipanema, Jacupiranga and Itatiaia in the Serra do Mar province. The Araxá, Salitre, Catalão I and Catalão II carbonatites are associated with cumulate rocks (e.g., apatitites, magnetitites and phlogopitites), dunites and wehrlites, whereas the Tapira carbonatites are associated with Ca-rich, Na-poor melilitite ± melilitolite ± ultramafic cumulate rocks (e.g., clinopyroxenites and "bebedourites"). On the other hand, the Jacupiranga carbonatites are associated with nephelinite ± melteigite/ijolite/urtite ± ultramafic cumulate rocks (e.g., pyroxenites), whereas the Ipanema carbonatites are associated with apatite-, magnetite- and phlogopite-bearing cumulate rocks. The Itatiaia complex is free from carbonatites and it is composed primarily of nepheline syenite grading to peralkaline varieties, quartz syenite, and granite (Melluso et al. 2017).

The 'carbonatites' field in Figure 7a is defined on the basis of micas analyzed in Catalão II and Catalão I carbonatites, which show a strong $^{[IV]}Fe^{3+}$ enrichment, slightly visible in micas from Ipanema carbonatites and absent in micas from Jacupiranga carbonatites (Figure 7b). In Figure 7b, phlogopite crystals analyzed in Sokli phoscorite-carbonatite complex (Finland; Lee et al. 2003) are plotted as comparison because they represent analyses of micas present in similar Catalão rocks. It is ~~well observable~~ as they ~~draws~~ the same trend observed for Catalão II phlogopite crystals. Slight Fe^{3+} enrichment is also visible in Alto Paranaíba kimberlites and kamafugites, particularly in Catalão II phlogopite-picrites that match the Catalão 'carbonatites' field (Figure 7c). Figure 7d compares micas belonging to several alkaline provinces, including those of Cenozoic rocks from Madagascar (Melluso and Morra 2000; Melluso et al. 2007; Cucciniello et al. 2011, 2016), Ischia Island in Italy (Melluso et al. 2014), the Jasra and Sung Valley complexes in India (Melluso et al. 2010, 2012) and Central

Mediterranean lamproites (Lepore et al. 2017). These micas follow the trend observed for the micas of the Serra do Mar Province, with lower Fe content associated with higher Si, Al and Mg contents.

Temperature, pressure and oxygen fugacity during the Catalão II mica crystallization

Igneous phlogopite crystallizes in a wide range of magmatic conditions (e.g., T, P, oxygen fugacity and chemical composition; Speer 1984). Several studies estimate crystallization T and P based on the partitioning of Al, Ti, and Ba in micas or between micas and liquid (e.g., Luhr et al. 1984; Righter and Carmichael 1996; Cesare et al. 2003; Henry et al. 2005; Uchida et al. 2007). However most of these relationships cannot be applied to Catalão micas, owing the low amounts or absence of Al, Ti and Ba. The temperature of Catalão II cumulate rocks (carbonatites, apatitites, magnetitites and phlogopitites) and Catalão II phlogopite-picrites can be estimated using the geothermometer of Luhr et al. (1984). This formula [$T\ (K) = 838/(1.0337\text{-}Ti/Fe^{2+})$] considers the ratio between octahedral Ti and Fe^{2+} (Table 6). The reliability of this formula was tested using published data for micas (Morogan and Wolley 1988; Brigatti et al. 1996; Seifert et al. 2000; Righter et al. 2002; Lee et al. 2003; Reguir et al. 2009; Bulchoz et al. 2014; Temizel et al. 2014; Ntomba et al. 2016; Pouclet et al. 2017; Lacalamita et al. 2017; Ivanov et al. 2018) where temperatures were determined independently (see results in the Supplemental[1] Table 2). The temperatures of micas in phlogopite-picrites estimated using the formula of Luhr et al. (1984) vary between 1050 and 952 °C, which is comparable with a primitive liquid formed directly from an enriched mantle, consistent with the temperature (900-1300 °C) reported by Righter and Carmichael (1996). Lower calculated temperatures (631-703 °C) for some mica may be justified as a late crystallization of groundmass micas. Micas from cumulate rocks show a slight to moderate variability in temperature, i.e., 1045 to 890 °C and 804 to 558 °C for calciocarbonatites, 806 to 571 °C for ferrocarbonatites, 786 to 647 °C for magnetitites, 932 to 587 °C for phlogopitites, and 689 and 594 °C for apatitites. These temperature ranges mirror different moments of mica crystallization during what

was likely a continuous process of fractional crystallization in a magma chamber. Higher temperatures (> 900 °C) are probably associated with an initial rapid cooling fractionation (as in Haynes et al. 2003). The range 500-800 °C is consistent with the fractionation temperature of the carbonatites and their related rocks (T = 750-550 °C in Haynes et al. 2003). The calculated temperatures in fenites vary between 754 and 586 °C, consistent with the temperature of Catalão II cumulate rocks that probably corresponds to the temperatures of fluids likely derived from the carbonatite intrusion. Catalão I micas show similar ranges of temperature, i.e., 742-542 °C for magnesiocarbonatites, 923-540 °C for magnetitites, and 679-550 °C for apatitites. Estimated temperatures are consistent with literature data, shown in Figure 6 of Cordeiro et al. 2011, where the isotopic composition of calcite is in equilibrium with apatite and magnetite in a temperature range of 800 to 500 °C. The empirical equation proposed by Uchida et al. (2007) [P(kb)= 3.03*^{T}Al-6.53(±0.33)] is not applicable for pressure assessment in Catalão micas because of their low tetrahedral ~~content in Al~~. Oxygen fugacity was evaluated using two different diagrams proposed in Wones and Eugster (1968): T (°C) vs. $Fe_{tot}/(Fe_{tot}+Mg)$ and $^{[IV]}Fe^{3+}$-$^{[VI]}Fe^{2+}$+ $^{[VI]}Fe^{3+}$-$^{[VI]}Mg$. Figures 8a and 8b indicate the oxidation state of the liquids from which the Catalão micas crystallized, and they illustrate mica behavior in the different rocks. The high Mg in Catalão micas is related primarily to the high oxygen fugacity that produces $Fe^{2+} \rightarrow Fe^{3+}$ transformation, ~~as also evidenced by~~ the contemporaneous crystallization of magnetite [assuming that $FeO_{(Phl)} << FeO_{(mt)}$] (Brigatti et al. 1996). The diagrams illustrated in Figures 8a and 8b show that Catalão II micas in calciocarbonatites, magnetitites and apatitites plot above the hematite - magnetite (HM) buffer. Micas in ferrocarbonatites, phlogopitites and phlogopite-picrites are consistent with two different oxygen fugacity: some plot between the NiNiO and HM buffers and others plot above the HM buffer. This different behavior is due to various moments of mica crystallization. The micas in fenites plot between HM-NiNiO buffers. All Catalão I micas in magnesiocarbonatites, magnetitites and apatitites plot above the HM buffer.

For both Catalão complexes, these diagrams illustrate the high oxidation state of the magma from which these micas crystallized. Further evidence is provided by magnetite-ilmenite pairs observed in a few Catalão samples. As shown in Figure 8c, their temperature values [640-571 °C in Catalão II calciocarbonatites; 862-564 °C in apatitites and 605-568 °C in magnetitites of Catalão I complex] are comparable with those estimated for micas in the same rocks. The magnetite-ilmenite pairs crystallized under HM-NiNiO conditions (see results in the Supplemental[1] Table 3), matching mica environment reasonably well.

ACKNOWLEDGEMENTS

Vincenza Guarino thanks Prof. Leone Melluso and Prof. Vincenzo Morra for their scientific guidance since her graduation thesis; she learned from them how to merge research, curiosity and methodological rigor to approach the various aspects of mineralogical, petrographic and petrologic studies. Thanks to Dott. Roberto de Gennaro for his invaluable help with the EDS analysis. The useful comments of Editor Keith D. Putirka helped very much to improve the manuscript. The comments of Prof. D.L. Bish have been useful to improve contents and style of the manuscript. The reviews of the Associate Editor Callum Hetherington, Technical Editor, Radek Škoda and an anonymous reviewer were very useful for the preparation of this revised manuscript. This research benefited from grants of Prof. Maria Franca Brigatti and from PRIN and Fondi Ricerca Dipartimentale to Prof. L. Melluso.

REFERENCES CITED LIST

Almeida, F.F.M., De Brito Neves, B.B., and Carneiro Dal Re, C. (2000) The origin and evolution of the south American platform. Earth Science Reviews, 50, 77–111.

Araújo, A.L.N., Carlson, R.W., Gaspar, J.C., and Bizzi, L.A. (2001) Petrology of kamafugites and kimberlites from the Alto Paranaíba Alkaline Province, Minas Gerais, Brazil. Contribution of Mineralogy and Petrology, 142, 163–177.

Arima, M., and Edgar, A.D. (1981) Substitution mechanisms and solubility of titanium in phlogopites from rocks of probable mantle origin. Contribution of Mineralogy and Petrology, 77, 288–295.

Bagdasarov, Yu.A., Vlasova, E.V., and Skosyreva, M.V. (1985) Typomorphism of micas in ultrabasic-alkaline rocks and carbonatites of the Maimecha-Kotui province. Izvestiya Akademii Nauk SSSR, Seriya Geologicheskaya, 6, 78–92.

Bailey, S.W. (1984) Crystal chemistry of the true micas. In S.W. Bailey, Ed., Micas, Reviews in Mineralogy, Mineralogical Society of America, Washington, D.C., 13, 13–60.

Biondi, J.C. (2005) Brazilian mineral deposits associated with alkaline and alkaline-carbonatite complexes. In P. Comin-Chiaramonti, and C.B. Gomes, Eds., Mesozoic to Cenozoic Alkaline Magmatism in the Brazilian Platform. FAPESP, São Paulo, Brazil, 707–750.

Brigatti, M.F., Medici, L., Saccani, E., and Vaccaro, C. (1996) Crystal chemistry and petrologic significance of Fe^{3+}- rich phlogopite from the Tapira carbonatite complex, Brazil. American Mineralogist, 81, 913–927.

Brigatti, M.F., Frigieri, P., Ghezzo, C., and Poppi, L. (2000a) Crystal chemistry of Al-rich biotites coexisting with muscovites in peraluminous granites. American Mineralogist, 85, 436–448.

Brigatti, M.F., Lugli, C., Poppi, L., Foord, E.E., and Kile, D.E. (2000b) Crystal chemical variations in Li- and Fe-rich micas from Pikes Peak Batholith (central Colorado). American Mineralogist, 85(9), 1275–1286.

Brigatti, M.F., Medici, L., Poppi, L., and Vaccaro, C. (2001) Crystal chemistry of trioctahedral micas-1M from Alto Paranaíba Igneous Province, Southeastern Brazil. Canadian Mineralogist, 39, 1333–1345.

Brigatti, M.F., and Guggenheim, S. (2002) Mica crystal chemistry and the influence of pressure, temperature, and solid solution on atomistic models. In A. Mottana, F.P. Sassi, J.B. Thompson Jr., and S. Guggenheim, Eds., Micas: crystal chemistry and metamorphic petrology, 499 pp. Reviews in Mineralogy and Geochemistry, Mineralogical Society of America, Washington, D.C.

Brigatti, M.F., Guggenheim, S., and Poppi, M. (2003) Crystal chemistry of the 1M mica polytype: The octahedral sheet. American Mineralogist, 88, 667–675.

Brigatti, M.F., Elmi, C., Guggenheim, S., Malferrari, D., and Poppi, M. (2016) An alternative method of calculating cleavage energy: the effect of compositional domains in micas. American Mineralogist, 101, 2738–2746.

Brod, J.A., Gibson, S.A., Thompson, R.N., Junqueira-Brod, T.C., Seer, H.J., De Moraes, L.C., and Boaventura, G.R. (2000) The kamafugite-carbonatite association in the Alto Paranaíba Igneous Province (APIP) southeastern Brazil. Revista Brasileira de Geociências, 30, 404–408.

Brod, J.A., Gaspar, J.C., Araújo, D.P., Gibson, S.A., Thompson, R.N., and Junqueira-Brod, T.C. (2001) Phlogopite and tetra-ferriphlogopite from Brazilian carbonatite complexes: petrogenetic constraints and implications for mineral-chemistry systematics. Journal of Asian Earth Science, 19, 265–296.

Bruker (2003) SMART and SAINT-Plus, version 6.01. Bruker AXS Inc., Madison, Wisconsin.

Bulchoz, C.E., Jagoutz, O., Schmidt, M.W., and Sambuu, O. (2014) Phlogopite- and clinopyroxene-dominated fractional crystallization of an alkaline primitive melt: petrology and mineral chemistry of the Dariv Igneous Complex, Western Mongolia. Contribution to Mineralogy and Petrology, 167, 994.

509 Cesare, B., Cruciani, G., and Russo, U. (2003) Hydrogen deficiency in Ti-rich biotite from anatectic
510 metapelites (El Joyazo, SE Spain): Crystal-chemical aspects and implications for high-temperature
511 petrogenesis. American Mineralogist, 88, 583–595.
512 Cordeiro, P.F.O., Brod, J.A., Santos, R.V., Dantas, E.L., Oliveira, C.G., and Barbosa, E.S.R. (2011)
513 Stable (C, O) and radiogenic (Sr, Nd) isotopes of carbonates as indicators of magmatic and post-
514 magmatic processes of phoscorite-series rocks and carbonatites from Catalão I, central Brazil.
515 Contribution to Mineralogy and Petrology, 161, 451–464.
516 Cucciniello, C. (2016) Tetra-Plot: A Microsoft Excel spreadsheet to perform tetrahedral diagrams.
517 Periodico di Mineralogia, 85(2), 115–119.
518 Cucciniello, C., Melluso, L., Morra, V., Storey, M., Rocco, I., Franciosi, L., Grifa, C., Petrone, C.M.,
519 and Vincent, M. (2011) New ^{39}Ar-^{40}Ar ages and petrogenesis of the Massif d'Ambre volcano,
520 northern Madagascar. In L. Beccaluva, G. Bianchini, and M. Wilson, Eds., Volcanism and
521 Evolution of the African Lithosphere. Geological Society of America Special Papers, 478, 257–
522 282.
523 Cucciniello, C., Tucker, R.D., Jourdan, F., Melluso, L., and Morra, V. (2016) The age and petrogenesis
524 of the alkaline magmatism of Ampasindava Peninsula and Nosy Be archipelago, northern
525 Madagascar. Mineralogy and Petrology, 110, 309–331.
526 Elmi, C., Brigatti, M.F., Guggenheim, S., Pasquali, L., Montecchi, M., and Nannarone, S. (2014)
527 Crystal chemistry and surface configurations of two iron-bearing trioctahedral mica-1*M* polytypes.
528 Clays and Clay Minerals, 62, 243–252.
529 Foley, S.F. (1989) Experimental constraints on phlogopite chemistry in lamproites: 1. The effect of
530 water activity and oxygen fugacity. European Journal of Mineralogy, 1, 411–426.
531 Gaspar, J.C., and Wyllie, P.J. (1982) Barium phlogopite from the Jacupiranga carbonatite, Brazil.
532 American Mineralogist, 67, 997–1000.

533 --- (1987) The phlogopites from the Jacupiranga carbonatite intrusions. Mineralogy and Petrology, 36,
534 121–134.
535 Gibson, S.A., Thompson, R.N., Leonardos, O.H., Dickin, A.P., and Mitchell, J.G. (1995) The late
536 Cretaceous impact of the Trindade Mantle Plume: evidence from large-volume, mafic, potassic
537 magmatism in SE Brazil. Journal of Petrology, 36, 189–229.
538 Gibson, S.A., Thompson, R.N., and Day, J.A. (2006) Timescales and mechanisms of plume-lithosphere
539 interactions: $^{40}Ar/^{39}Ar$ geochronology and geochemistry of alkaline igneous rocks from the Paraná
540 - Etendeka large igneous province. Earth and Planetary Science Letters, 251, 1–17.
541 Gomes, C.B., and Comin-Chiaramonti, P. (2005) Some notes on the Alto Paranaíba igneous province.
542 In P. Comin-Chiaramonti, and C.B. Gomes, Eds., Mesozoic to Cenozoic Alkaline Magmatism in
543 the Brazilian Platform. FAPESP, São Paulo, Brazil, 317–340.
544 Greenwood, J.C. (1998) Barian-titanian micas from Ilha da Trindade, South Atlantic. Mineralogical
545 Magazine, 62, 687–695.
546 Guarino, V., Azzone, R.G., Brotzu, P., Gomes, C.B., Melluso, L., Morbidelli, L., Ruberti, E., Tassinari,
547 C.C.G., and Brilli, M. (2012) Magmatism and fenitization in the Cretaceous potassium-alkaline-
548 carbonatitic complex of Ipanema São Paulo State, Brazil. Mineralogy and Petrology, 104, 43–61.
549 Guarino, V., Wu, F.Y., Lustrino, M., Melluso, L., Brotzu, P., Gomes, C.B., Ruberti, E., Tassinari,
550 C.C.G., and Svisero, D.P. (2013) U-Pb ages, Sr-Nd- isotope geochemistry, and petrogenesis of
551 kimberlites, kamafugites and phlogopite-picrites of the Alto Paranaíba Igneous Province, Brazil.
552 Chemical Geology, 353, 65–82.
553 Guarino, V., Wu, F.Y., Melluso, L., Gomes, C.B., Tassinari, C.C.G., Ruberti, E., and Brilli, M. (2017)
554 U-Pb ages, geochemistry, C-O-Nd-Sr-Hf isotopes and petrogenesis of the Catalão II carbonatitic
555 complex (Alto Paranaíba Igneous Province, Brazil): implications for regional-scale heterogeneities

556 in the Brazilian carbonatite associations. International Journal of Earth Sciences (Geol Rundsch),
557 106(6), 1963–1989.
558 Guimarães, H.N., and Weiss, R.A. (2013) The complexity of the niobium deposits in the alkaline
559 ultramafic intrusions Catalão I and II – Brazil.
560 www.cbmm.com.br/portug/sources/techlib/science/pdfs/002A.pdf.
561 Haynes, E.A., Moecher, D.P., and Spicuzza, M.J. (2003) Oxygen isotope composition of carbonates,
562 silicates, and oxides in selected carbonatites: constraints on crystallization temperatures of
563 carbonatite magmas. Chemical Geology, 193, 43–57.
564 Henry, D.J., Guidotti, C.V., and Thomson, J.A. (2005) The Ti saturation surface for low-to-medium
565 pressure metapelitic biotites: Implications for geothermometry and Ti-substitution mechanisms.
566 American Mineralogist, 90, 316–328.
567 Heathcote, R.C., and McCormick, G.R. (1989) Major-cation substitution in phlogopite and evolution of
568 carbonatite in the Potash Sulphur Springs complex, Garland County, Arkansas. American
569 Mineralogist, 74, 132–140.
570 Ivanov, A.V., Demonterova, E.I., Savatenkov, V.M., Perepelov, A.B., Ryabov, V.V., and Shevko, A.Y.
571 (2018) Late Triassic (Carnian) lamproites from Noril'sk, polar Siberia: Evidence for melting of the
572 recycled Archean crust and the question of lamproite source for some placer diamond deposits of
573 the Siberian Craton. Lithos, 296-299, 67–78.
574 Kamenetsky, V.S., Kamenetsky, M.B., Weiss, Y., Navon, O., Nielsen, T.F.D., and Mernagh, T.P.
575 (2009) How unique is the Udachnaya-East kimberlite? Comparison with kimberlites from the
576 Slave Craton (Canada) and SW Greenland. Lithos, 112, 334–346.
577 Krasnova, N.I. (2001) The Kovdor phlogopite deposit, Kola Peninsula, Russia. Canadian Mineralogist,
578 39, 33–44.

579 Krivdik, S.G., Glevasskii, E.B., and Levina, R.L. (1982) Composition of magnesian-ferroan micas of
580 the Chernigov carbonatite complex [USSR]. Mineralogicheskii Zhurnal, 4, 78–85.
581 Lacalamita, M., Schingaro, E., Scordari, F., Ventruti, G., Fabbrizio, A., and Pedrazzi, G. (2011)
582 Substitution mechanisms and implications for the estimate of water fugacity for Ti-rich phlogopite
583 from Mt. Vulture (Potenza, Italy). American Mineralogist, 96, 1381–1391.
584 Lacalamita, M., Balassone, G., Schingaro, E., Mesto, E., Mormone, A., Piochi, M., Ventruti, G.,
585 Joachimski, M., and Grew, E. (2017) Fluorophlogopite-bearing and carbonate metamorphosed
586 xenoliths from the Campanian Ignimbrite (Fiano, southern Italy): crystal chemical, geochemical
587 and volcanological insights. Mineralogical Magazine, 81(5), 1165–1189.
588 Laurora, A., Brigatti, M.F., Mottana, A., Malferrari, D., and Caprilli, E. (2007) Crystal chemistry of
589 trioctahedral micas in alkaline and subalkaline volcanic rocks: A case study from Mt. Sassetto
590 (Tolfa district, Latium, central Italy). American Mineralogist, 92, 468–480.
591 Le Bas, M.J. (2008) Fenites associated with carbonatites. Canadian Mineralogist, 46, 915–932.
592 Lee, M.J., Garcia, D., Moutte, J., and Lee, J.I. (2003) Phlogopite and tetraferriphlogopite from
593 phoscorite and carbonatite associations in the Sokli massif, Northern Finland. Geosciences Journal,
594 7(1), 9–20.
595 Lepore, G.O., Bindi, L., Pedrazzi, G., Conticelli, S., and Bonazzi, P. (2017) Structural and chemical
596 variations in phlogopite from lamproitic rocks of the Central Mediterranean region. Lithos, 286-
597 287, 191–205.
598 Luhr, J.F., Carmichael, I.S.E., and Varekamp, J.C. (1984) The 1982 eruptions of El Chichón Volcano,
599 Chiapas, Mexico: Mineralogy and petrology of the an hydrate bearing pumices. Journal of
600 Volcanology and Geothermal Research, 23, 69–108.
601 Machado, D.L. (1991) Geologia e aspectos metalogenéticos do complexo alcalino-carbonatitico de
602 Catalão II (GO), thèse, Universidade Estadual de Campinas (SP), Brésil, 102 pp.

603 Mantovani, M.S.M., Louro, V.H.A., Ribeiro, V.B., Requejo, H.S., and dos Santos, R.P.Z. (2016)
604 Geophysical analysis of Catalão I alkaline–carbonatite complex in Goiás, Brazil. Geophysical
605 Prospecting, 36, 216–227.
606 Melluso, L., and Morra, V. (2000) Petrogenesis of late Cenozoic mafic alkaline rocks of the Nosy Be
607 archipelago (northern Madagascar): relationships with the Comorean magmatism. Journal of
608 Volcanology and Geothermal Research, 56, 129–142.
609 Melluso, L., Morra, V., Riziky, H., Veloson, J., Lustrino, M., Del Gatto, L., and Modeste, V. (2007)
610 Petrogenesis of a basanite-tephrite-phonolite volcanic suite in the Bobaomby (Cap d'Ambre)
611 peninsula, northern Madagascar. Journal of African Earth Sciences, 49, 29–42.
612 Melluso, L., Lustrino, M., Ruberti, E., Brotzu, P., Gomes, C.B., Morbidelli, L., Morra, V., Svisero,
613 D.P., and d'Amelio, F. (2008) Major- and trace-element composition of olivine, perovskite,
614 clinopyroxene, Cr-Fe-Ti oxides, phlogopites and host kamafugites and kimberlites, Alto Paranaíbá,
615 Brazil. Canadian Mineralogist, 46, 19–40.
616 Melluso, L., Srivastava, R.K., Guarino, V., Zanetti, A., and Sinha, A.K. (2010) Mineral compositions
617 and magmatic evolution of the Sung Valley ultramafic-alkaline-carbonatitic complex (NE India).
618 Canadian Mineralogist, 48, 205–229.
619 Melluso, L., Srivastava, R.K., Petrone, C.M., Guarino, V., and Sinha, A.K. (2012) Mineralogy and
620 magmatic affinity of the Jasra clinopyroxenitic-gabbroic-syenitic complex, Shillong Plateau,
621 northeastern India. Mineralogical Magazine, 76(5), 1099–1117.
622 Melluso, L., Morra, V., Guarino, V., de Gennaro, R., Franciosi, L., and Grifa, C. (2014) The
623 crystallization of shoshonitic to peralkaline trachyphonolitic magmas in a H_2O-Cl-F-rich
624 environment at Ischia (Italy), with implications for the feeder system of the Campania Plain
625 volcanoes. Lithos, 210-211, 242–259.

626 Melluso, L., Guarino, V., Lustrino, M., Morra, V., and de Gennaro, R. (2017) The REE- and HFSE-
627 bearing phases in the Itatiaia alkaline complex (Brazil), and geochemical evolution of feldspar-rich
628 felsic melts. Mineralogical Magazine, 81(2), 217–250.
629 Meyrowitz, R. (1970) New semi-microprocedure for determination of ferrous iron in refractory silicate
630 minerals using a sodium metafluoborate decomposition. Analytical Chemistry, 42, 1110–1113.
631 Mitchell, R.H. (1995) Kimberlites, Orangeites and Related Rocks. Plenum Press, New York.
632 Mitchell, R.H. (2005) Carbonatites and carbonatites and carbonatites. Canadian Mineralogist, 43,
633 2049–2068.
634 Mitchell, R.H., and Bergman, S.C. (1991) Petrology of Lamproites. Plenum Press, New York.
635 Morbidelli, L., Gomes, C.B., Beccaluva, L., Brotzu, P., Garbarino, C., Riffel, B.F., Ruberti, E., and
636 Traversa, G. (1997) Parental magma characterization of Salitre cumulate rocks (Alto Paranaíba
637 Alkaline Province, Brazil) as inferred from mineralogical, petrographic, and geochemical data.
638 International Geology Reviews, 39, 723–743.
639 Morogan, V., and Wolley, A.R. (1988) Fenitization at the Alnö carbonatite complex, Sweden;
640 distribution, mineralogy and genesis. Contribution to Mineralogy and Petrology, 100, 169–182.
641 Naemura, K., Hirajima, T., and Svojtka, M. (2009) The pressure-temperature path and the origin of
642 phlogopite in spinel-garnet peridotites from the Blansky Les Massif of the Moldanubian Zone,
643 Czech Republic. Journal of Petrology, 50, 1795–1827.
644 Ntomba, A.M., Bidzang, F.N., Ottou, J.E.M., Ngalamo, F.J.G., Bisso, D., Takamte, C.R.M., and
645 Ondoa, J.M. (2016) Phlogopite compositions as an indicator of both the geodynamic context of
646 granitoids and the metallogeny aspect in Memve'ele Archean area, northwestern Congo craton.
647 Journal of African Earth Sciences, 118, 231–244.
648 Pouclet, A., El Hadi, H., Bardintzeff, J.-M., Benharref, M., and Fekkak, A. (2017) Devonian to Early
649 Carboniferous magmatic alkaline activity in the Tafilalt Province, Eastern Morocco: An

650 Eovariscan episode in the Gondwana margin, north of the West African Craton. Journal of African
651 Earth Sciences, 129, 814–841.
652 Read, G., Grutter, H., Winter, S., Luckman, N., Gaunt, F., and Thomsen, F. (2004) Stratigraphic
653 relations, kimberlite emplacement and lithospheric thermal evolution, Quiricò Basin, Minas Gerais
654 State, Brazil. Lithos, 77, 803–818.
655 Reguir, E.P., Chakhmouradian, A.R., Halden, N.M., Malkovets, V.G., and Yang, P. (2009) Major- and
656 trace-element compositional variation of phlogopite from kimberlites and carbonatites as a
657 petrogenetic indicator. Lithos, 112S1, 372–384.
658 Riccomini, C., Velázquez, V.F., and Gomes, C.B. (2005) Tectonic controls of the Mesozoic and
659 Cenozoic alkaline magmatism in the central-southeastern Brazil Platform. In P. Comin-
660 Chiaramonti, and C.B. Gomes, Eds., Mesozoic to Cenozoic Alkaline Magmatism in the Brazilian
661 Platform. FAPESP, São Paulo, Brazil, 31–55.
662 Righter, K., and Carmichael, I.S.E. (1996) Phase equilibria of phlogopite lamprophyres from western
663 Mexico: biotite-liquid equilibria and P-T estimates for biotite-bearing igneous rocks. Contributions
664 to Mineralogy and Petrology, 123, 1–21.
665 Righter, K., Dyar, M.D., Delaney, J.S., Vennemann, T.W., Hervig, R.L., and King, P.L. (2002)
666 Correlations of octahedral cations with OH^-, O_2^-, Cl^-, and F^- in biotite from volcanic rocks and
667 xenoliths. American Mineralogist, 87, 142–153.
668 Rocha, E., Nasraoui, M., Soubiès, F., Bilal, E., and Perseval, P. (2001) Évolution géochimique du
669 pyrochlore au cours de l'altération météorique du gisement de Catalão II (Goiás, Brésil). Comptes
670 Rendus de l'Académie des Sciences, 332, 91–98.
671 Schingaro, E., Lacalamita, M., Scordari, F., Brigatti, M.F., and Pedrazzi, G. (2011) Crystal chemistry
672 of Ti-rich fluorophlogopite from Presidente Olegario, Alto Paranaíba igneous province, Brazil.
673 American Mineralogist, 96, 732–743.

Schingaro, E., Kullerud, K., Lacalamita, M., Mesto, E., Scordari, F., Zozulya, D., Erambert, M., and Ravna, E.J.K. (2014) Yangzhumingite and phlogopite from the Kvaløya lamproite (North Norway): Structure, composition and origin. Lithos, 210-211, 1–13.

Scordari, F., Schingaro, E., Ventruti, G., Nicotra, E., Viccaro, M., and Mazziotti Tagliani, S. (2013) Fluorophlogopite from Piano delle Concazze (Mt. Etna, Italy): crystal chemistry and implications for the crystallization conditions. American Mineralogist, 98, 1017–1025.

Seifert, W., Kämpf, H., and Wasternack, J. (2000) Compositional variation in apatite, phlogopite and other accessory minerals of the ultramafic Delitzsch complex, Germany: implication for cooling history of carbonatites. Lithos, 53, 81–100.

Shannon, R.D. (1976) Revised effective ionic radii and systematic studies of interatomic distances in halides and chalcogenides. Acta Crystallographica, A32, 751–767.

Sheldrick, G.M. (1996) SADABS. University of Göttingen, Germany.

--- (1997) SHELXL97. Program for the Refinement of Crystal Structures. University of Göttingen, Germany.

Signorelli, S., Vaggelli, G., and Romano, C. (1999) Pre-eruptive volatile (H_2O, F, Cl, and S) contents of phonolitic magmas feeding the 3550-year old Avellino eruption from Vesuvius, southern Italy. Journal of Volcanology and Geothermal Research, 93, 237–256.

Speer, J.A. (1984) Micas in igneous rocks. In S.W. Bailey, Ed., Micas, Mineralogical Society of America Reviews in Mineralogy, 13, 229–356.

Temizel, İ., Arslan, M., Abdioğlu, E., and Yücel, C. (2014) Mineral chemistry and thermobarometry of Eocene monzogabbroic stocks from the Bafra (Samsun) area in Turkey: implications for disequilibrium crystallization and emplacement conditions. International Geology Review, 56(10), 1226–1245.

Tischendorf, G., Rieder, M., Förster, H.-J., Gottesmann, B., and Guidotti, C.V. (2004) A new graphical presentation and subdivision of potassium micas. Mineralogical Magazine, 68, 649–667.

Tischendorf, G., Förster, H.-J., Gottesmann, B., and Rieder, M. (2007) True and brittle micas: composition and solid-solution series. Mineralogical Magazine, 71, 285–320.

Traversa, G., Gomes, C.B., Brotzu, P., Buraglini, N., Morbidelli, L., Principato, M.S., Ronca, S., and Ruberti, E. (2001) Petrography and mineral chemistry of carbonatites and mica-rich rocks from the Araxá complex (Alto Paranaíba Province, Brazil). Anais da Academia Brasileira de Ciências, 73, 71–98.

Uchida, E., Endo, S., and Makino, M. (2007) Relationship between solidification depth of granitic rocks and formation of hydrothermal ore deposits. Resource Geology, 57, 47–56.

Whitney, D.L., and Evans, B.W. (2010) Abbreviations for names of rock-forming minerals. American Mineralogist, 95, 185–187.

LIST OF FIGURE CAPTIONS

Figure 1. Location with U–Pb ages of the Catalão I ([I]Guarino et al. 2017) and Catalão II ([II]Guarino et al. 2013) alkaline-carbonatite complexes in Brazil. The alkaline provinces of the central-southeastern region of the Brazilian Platform, and their relationships to major structural features are also shown (after Riccomini et al. 2005 and Melluso et al. 2017): 1) Late Ordovician to Early Cretaceous Paraná Basin; 2) Early Cretaceous tholeiitic lava flows; 3) Late Cretaceous Bauru Basin; 4) alkaline complexes associated with carbonatites; 5) alkaline complexes without associated carbonatites (age: diamonds, Permian-Triassic; squares, Early Cretaceous; triangles, Late Cretaceous; circles, Paleogene); 6) Axes of main arcs (AX, Alto Xingu; SV, São Vicente; BJ, Bom Jardim de Goiás; PG, Ponta Grossa; RG, Rio Grande; PP, Ponta Porã); 7) Torres Syncline; 8) Major fracture zones, in part deep lithospheric faults (Rifts: MR, Mercedes; RM, Rio das Mortes; MG, Moirão; SR, Santa Rosa; AR, Asunción; Lineaments: TB, Transbrasiliano; MJ, Moji-Guaçu; CF, Cabo Frio; RT, Rio Tietê; SL, São Carlos-Leme; PR, Paranapanema; PI, Piedade; GP, Guapiara; JC, São Jerônimo-Curiúva; RA, Rio Alonzo; PQ, Rio Piquiri; AM, Santa Lucia-Aiguá-Merin). *Inset* shows the location of the Paraná Basin CFB (Continental Flood Basalts), the São Francisco Craton, Trindade Island and the Alto Paranaíba Igneous Province.

Figure 2. a) $^{[IV]}Si$ vs. $^{[IV]}Al$ and b) $^{[IV]}Fe^{3+}$ vs. $^{[IV]}Al$ for Catalão phlogopite and ferriphlogopite crystals. The number of atoms per formula unit (apfu) was calculated following the normalization procedure presented in the Experimental section as reported in Table 2.

Figure 3. Catalão micas in the classification diagram after Tischendorf et al. (2007): $feal = {}^{[VI]}(Fe_{total} + Mn + Ti - Al)$ vs. $mgli = {}^{[VI]}(Mg - Li)$. Samples and symbols as in Figure 2.

Figure 4. Micas from Catalão I and Catalão II complexes: (a) $^{[VI]}Ti$ vs. $^{[VI]}Mg$ for Catalão phlogopite and ferriphlogopite crystals; (b) ⟨O3-O3⟩ unshared octahedral edges vs. the area defined by tetrahedral oxygen atoms ($^{[IV]}\langle O\text{-}O\rangle_{basal}$); (c) $^{[IV]}\langle O\text{-}O\rangle_{basal}$ vs. octahedral $^{[VI]}Mg$ content; and (d) relationships

between tetrahedral and octahedral charge (e^- apfu). Samples and symbols as in Figure 2. Data for phlogopite and tetraferriphlogopite of Tapira and Alto Paranaíba kamafugites are from Brigatti et al. (1996, 2001), Elmi et al. (2014) and Schingaro et al. (2011).

Figure 5. (a) Relationships between $(OH)^-$ content in the O4 site and $^{[VI]}$Ti content. (b) Variation of the distance between interlayer cation (A) and anionic O4 site with $^{[VI]}$Ti content.

Figure 6. Relationships between *a* and *c* unit-cell parameters.

Figure 7. Tetraplot diagram reporting the main tetrahedral [$^{[IV]}$Si (/3), $^{[IV]}$Al (*2) and $^{[IV]}Fe^{3+}$ (*3)] and octahedral $^{[VI]}$Mg cations used to compare micas of Catalão II and Catalão I rock (this work) with those of other alkaline districts, such as Tapira (Brigatti et al. 1996), Salitre (Morbidelli et al. 1997), Araxá (Traversa et al. 2001) in the Alto Paranaíba Igneous Province (Brazil), Ipanema (Guarino et al. 2012), Jacupiranga (Gaspar and Wyllie 1982, 1987; Brod et al. 2001), Itatiaia (Melluso et al. 2017) in the Serra do Mar (Brazil), Sokli complex (Finland; Lee et al. 2003); Cenozoic Madagascar rocks (Melluso and Morra 2000; Melluso et al. 2007; Cucciniello et al. 2011, 2016), Ischia Island in Italy (Melluso et al. 2014), Jasra and Sung Valley complexes in India (Melluso et al. 2010, 2012) and Central Mediterranean lamproites (Lepore et al. 2017). The tetrahedral diagram was prepared using the Tetra-Plot spreadsheet (Cucciniello 2016).

Figure 8. a) T (°C) vs. $Fe_{tot}/(Fe_{tot}+Mg)$ and b) $^{[IV]}Fe^{3+}$-$^{[VI]}Fe^{2+}$+ $^{[VI]}Fe^{3+}$-$^{[VI]}$Mg diagrams (Wones and Eugster 1968) used to estimate the environment oxygen fugacity during mica crystallization; c) log fO_2 vs. T(°C) for some Catalão magnetite-ilmenite pairs.

LIST OF TABLE CAPTIONS

Table 1. Modal analyses and mica types of the main rocks from the Catalão II and Catalão I complexes.

Table 2. Averaged major element analyses (oxide wt%), standard deviations and chemical formulae of mica crystals from representative thin sections of Catalão II and Catalão I. Analyses and chemical

formulae of crystals coming from the same thin section but showing remarkable differences in their compositions were not averaged or were averaged over compositionally homogeneous subgroups.

Table 3. Major element analyses (oxide wt%) and chemical formulae of mica crystals from Catalão II and Catalão I complexes used in single-crystal X-ray diffraction study.

Table 4. Relevant cation-anion bond lengths for Catalão II and Catalão I 1M micas.

Table 5. The $^{[IV]}Fe^{3+}$ variation in phlogopite crystals related to their drill-core depth in the Catalão II and Catalão I rocks.

Table 6. Range of temperature estimated for phlogopite crystals for Catalão II and Catalão I rocks and those obtained for a few Catalão magnetite-ilmenite pairs.

SUPPLEMENTAL MATERIALS

Supplemental[1] Figure 1. Representative thin section photomicrographs of Catalão I rocks. Abbreviations: MgCc, magnesiocarbonatite; phl, phlogopite; opq, opaque mineral; pcl, pyrochlore; ap, apatite; dol, dolomite; mgs, magnesite (Whitney and Evans 2010).

Supplemental[1] Figure 2. Representative thin section photomicrographs of Catalão II rocks. Abbreviations: CaCc, calciocarbonatite; FeCc, ferrocarbonatite; amp, amphibole; ap, apatite; cal, calcite; cpx, clinopyroxene; opq, opaque mineral; pcl, pyrochlore; phl, phlogopite; prv, perovskite; wad, wadeite (Whitney and Evans 2010).

Supplemental[1] Figure 3. Many TiO_2 vs. Al_2O_3 and TiO_2 vs. MgO (in wt%) diagrams, where each one compares mica compositions with their related host rocks. To comparison are reported also carbonates and opaque minerals (data taken from Guarino et al. 2017).

Supplemental[1] Table 1. Additional compositional data for Catalão II and Catalão I phlogopite crystals, determined with an energy dispersive spectrometer (EDS) at Dipartimento di Scienze della Terra, dell'Ambiente e delle Risorse (Di.S.T.A.R.), University of Napoli Federico II.

782 **Supplemental[1] Table 2**. Evaluation of mica temperature reliability using formula proposed by Luhr et

783 al. (1984).

784 **Supplemental[1] Table 3**. Composition of Catalão magnetite-ilmenite samples.

785 **CIF file**: CIF FILES CATALAO PHL.

786

787 **Endnotes:**

788 [1] Deposit Item AM-xx-yyy, Supplemental[1] Tables, Supplemental[1] Figures and CIF file. Deposit items

789 may also be available on the American Mineralogist web at http://www.minsocam.org.

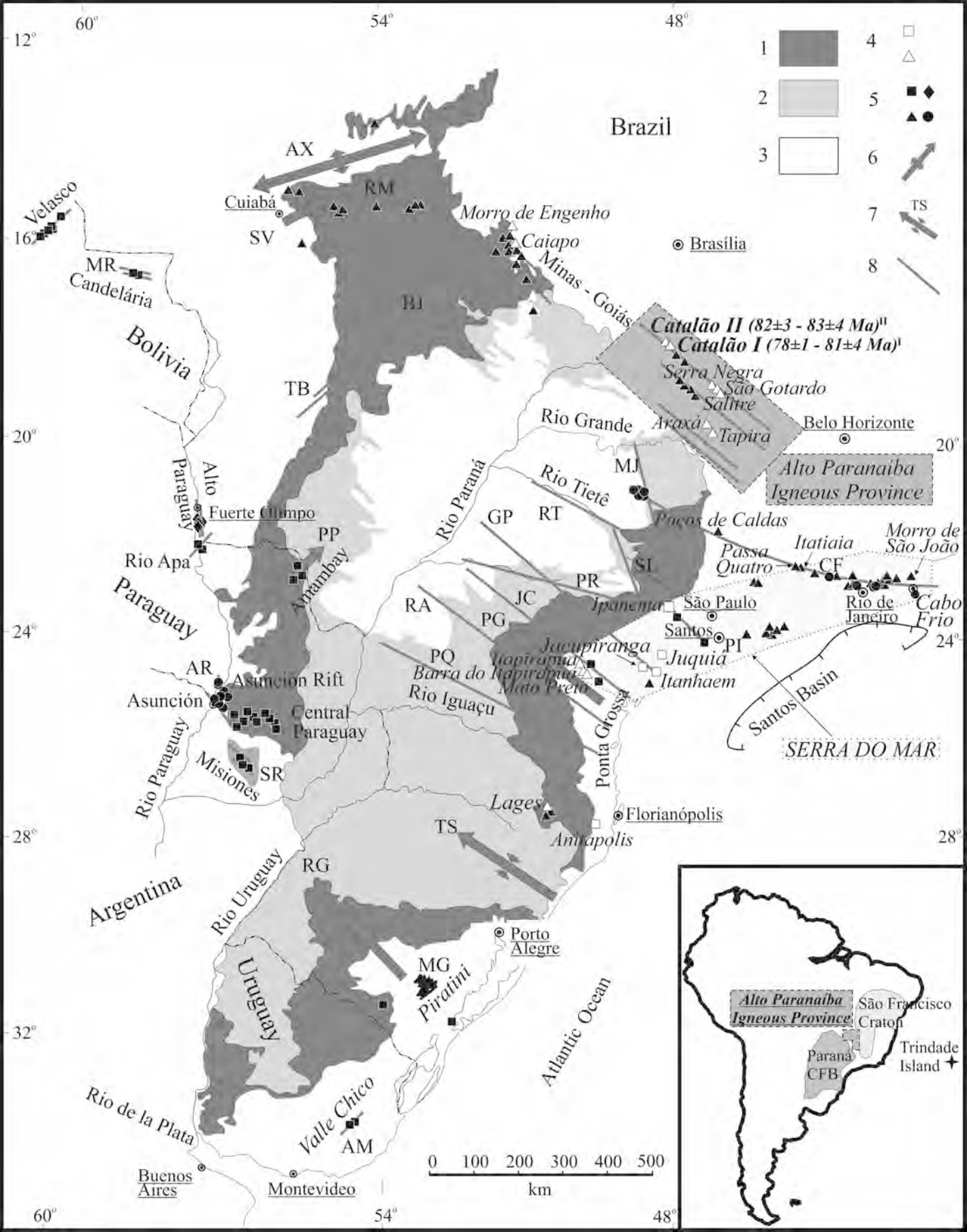
60°
54°
48°
12°
16°
20°
24°
28°
32°
1
2
3
4
5
6
7
8
TS
Brazil
AX
RM
Cuiabá
SV
Morro de Engenho
Caiapo
Minas - Goiás
Brasília
Velasco
MR
Candelária
BJ
Bolivia
Catalão II (82±3 - 83±4 Ma)II
Catalão I (78±1 - 81±4 Ma)I
Serra Negra
São Gotardo
Salitre
Araxá
Tapira
Belo Horizonte
TB
Rio Grande
Alto Paranaiba Igneous Province
MJ
Rio Tietê
Rio Paraná
Alto Paraguay
Fuerte Olimpo
GP
RT
Poços de Caldas
Morro de São João
Itatiaia
Passa Quatro
CF
SL
PP
Rio Apa
Amambay
PR
RA
JC
Ipanema
São Paulo
Rio de Janeiro
Cabo Frio
Paraguay
PG
Santos
PI
Jacupiranga
Juquiá
PQ
Itapirapuã
Barra do Itapirapuã
Itanhaem
AR
Asunción Rift
Asunción
Rio Iguaçu
Central Paraguay
Santos Basin
Rio Paraguay
Misiones
SR
Ponta Grossa
SERRA DO MAR
Lages
Florianópolis
TS
Anitapolis
RG
Argentina
Rio Uruguay
Porto Alegre
MG
Piratini
Uruguay
Atlantic Ocean
Rio de la Plata
Valle Chico
AM
Buenos Aires
Montevideo
0 100 200 300 400 500
km
Alto Paranaiba Igneous Province
São Francisco Craton
Paraná CFB
Trindade Island

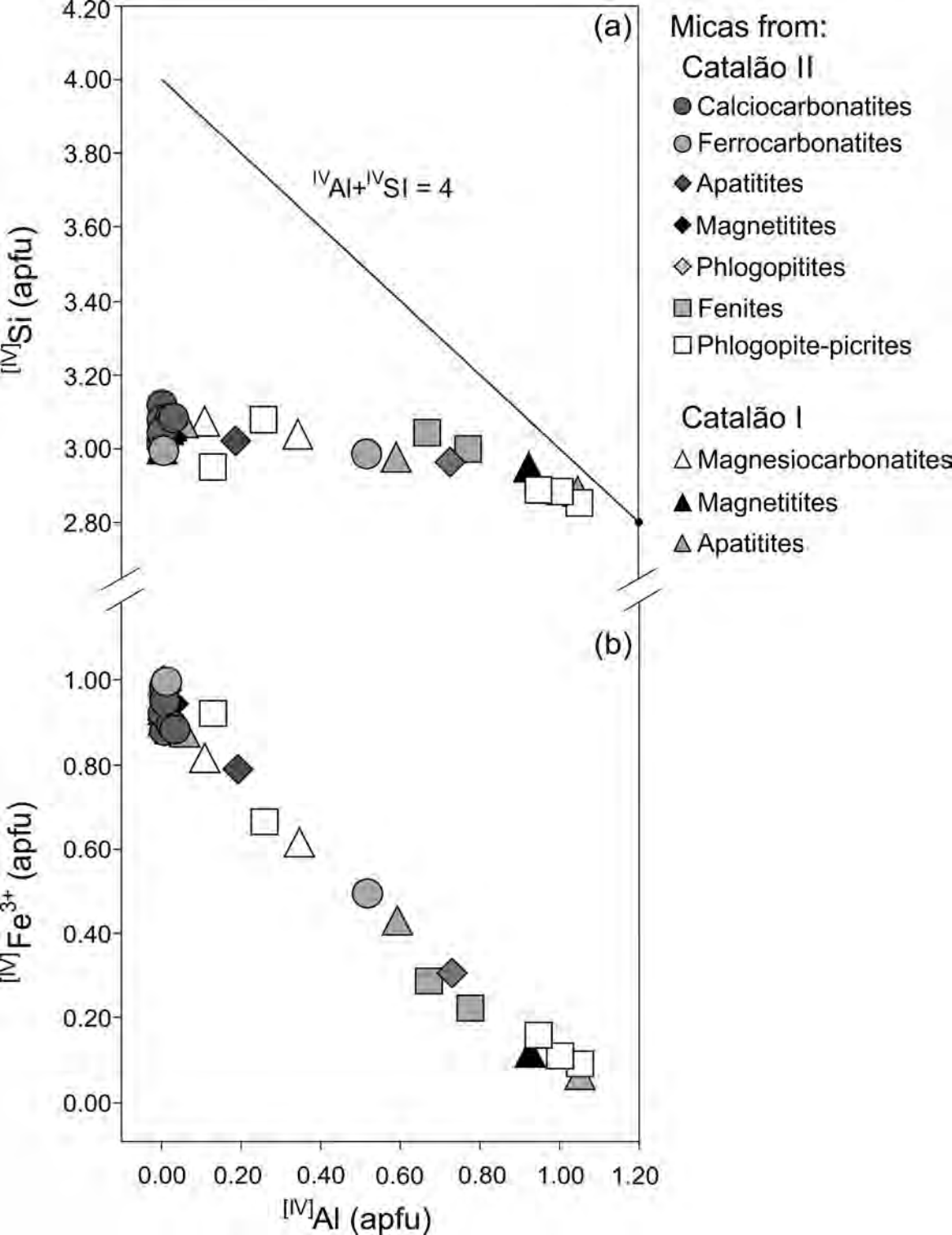
(a)
(b)
Micas from:
Catalão II
Calciocarbonatites
Ferrocarbonatites
Apatitites
Magnetitites
Phlogopitites
Fenites
Phlogopite-picrites
Catalão I
Magnesiocarbonatites
Magnetitites
Apatitites
$^{IV}Al+^{IV}SI = 4$
$^{[IV]}Si$ (apfu)
$^{[IV]}Fe^{3+}$ (apfu)
$^{[IV]}Al$ (apfu)
4.20
4.00
3.80
3.60
3.40
3.20
3.00
2.80
1.00
0.80
0.60
0.40
0.20
0.00
0.00
0.20
0.40
0.60
0.80
1.00
1.20

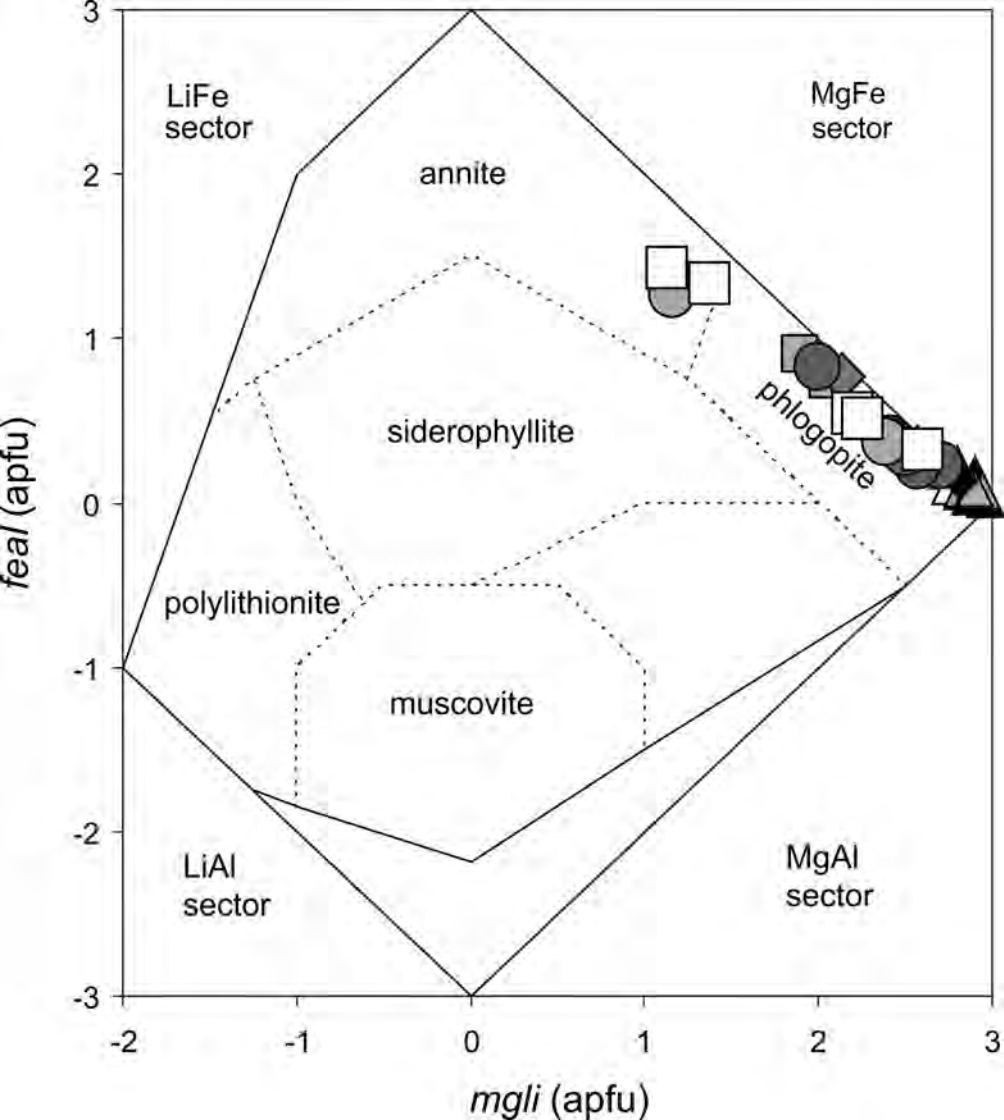
LiFe sector
MgFe sector
annite
siderophyllite
phlogopite
polylithionite
muscovite
LiAl sector
MgAl sector
3
2
1
0
-1
-2
-3
-2
-1
0
1
2
3
feal (apfu)
mgli (apfu)

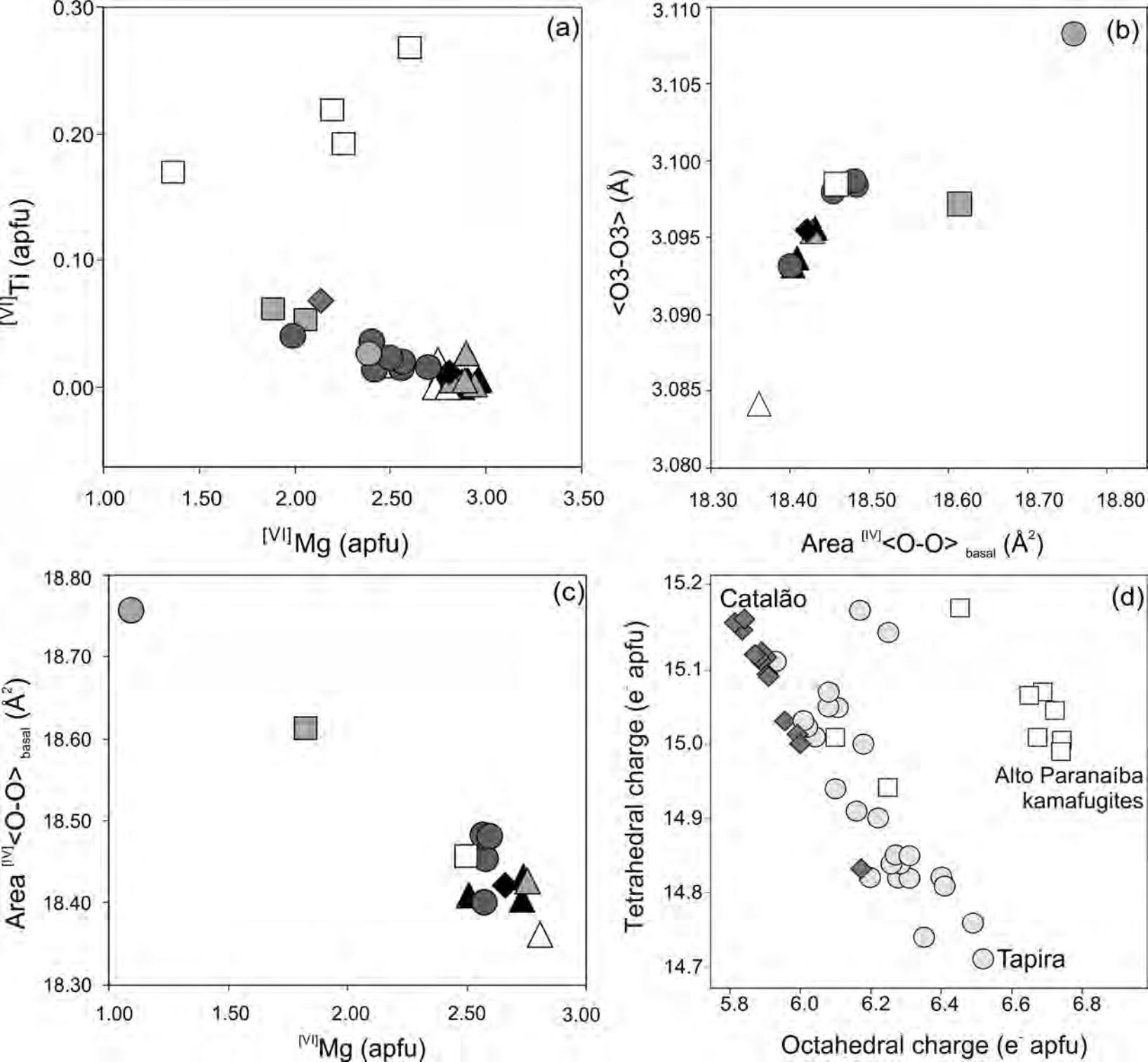
(a)
[VI]Ti (apfu)
[VI]Mg (apfu)
0.30
0.20
0.10
0.00
1.00
1.50
2.00
2.50
3.00
3.50
(b)
<O3-O3> (Å)
Area [IV]<O-O> basal (Å²)
3.110
3.105
3.100
3.095
3.090
3.085
3.080
18.30
18.40
18.50
18.60
18.70
18.80
(c)
Area [IV]<O-O> basal (Å²)
[VI]Mg (apfu)
18.80
18.70
18.60
18.50
18.40
18.30
1.00
1.50
2.00
2.50
3.00
(d)
Catalão
Alto Paranaíba kamafugites
Tapira
Tetrahedral charge (e⁻ apfu)
Octahedral charge (e⁻ apfu)
15.2
15.1
15.0
14.9
14.8
14.7
5.8
6.0
6.2
6.4
6.6
6.8

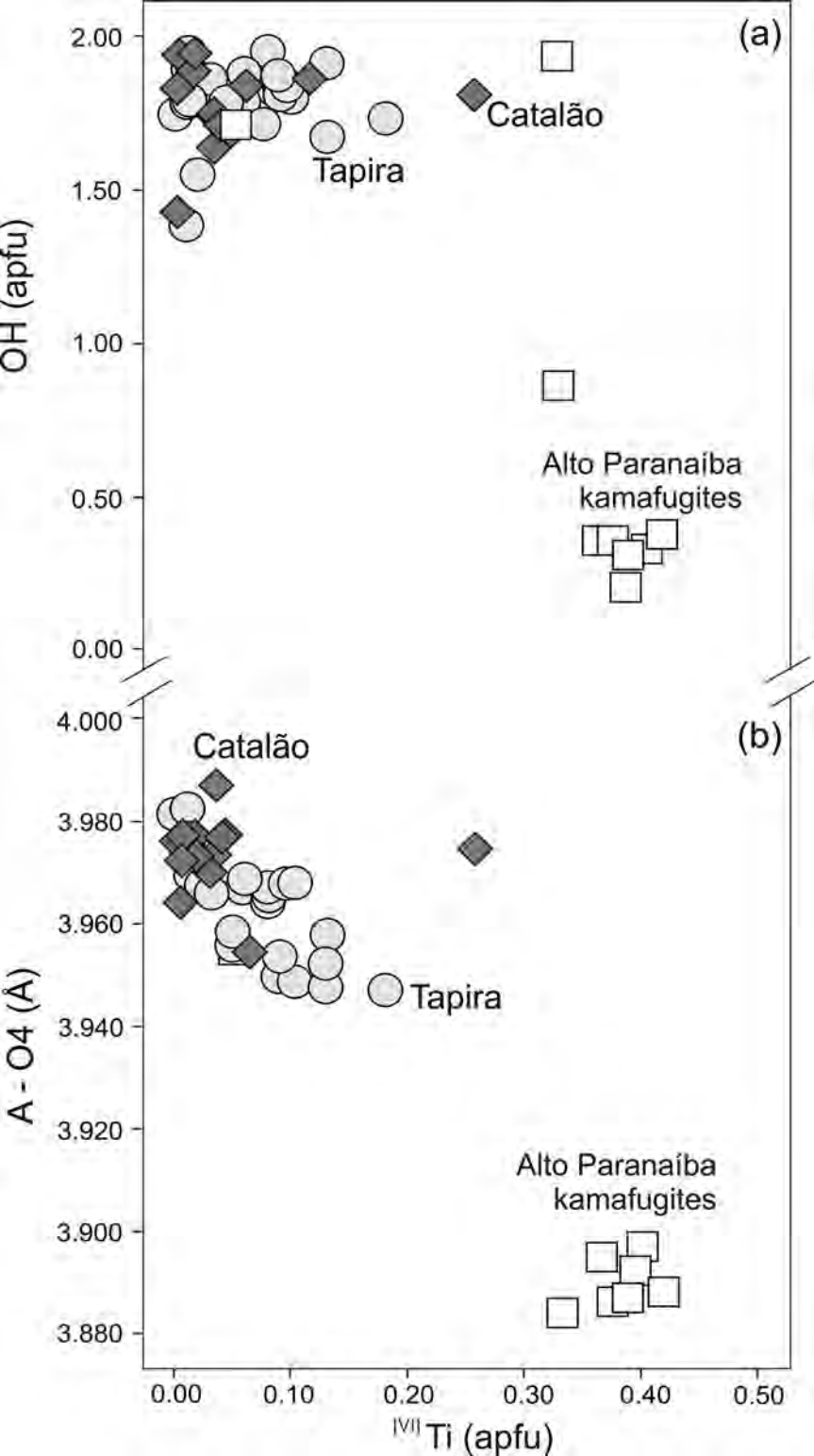
(a)
2.00
1.50
1.00
0.50
0.00
OH (apfu)
Catalão
Tapira
Alto Paranaíba
kamafugites
(b)
4.000
3.980
3.960
3.940
3.920
3.900
3.880
A - O4 (Å)
Catalão
Tapira
Alto Paranaíba
kamafugites
0.00
0.10
0.20
0.30
0.40
0.50
[VI]Ti (apfu)

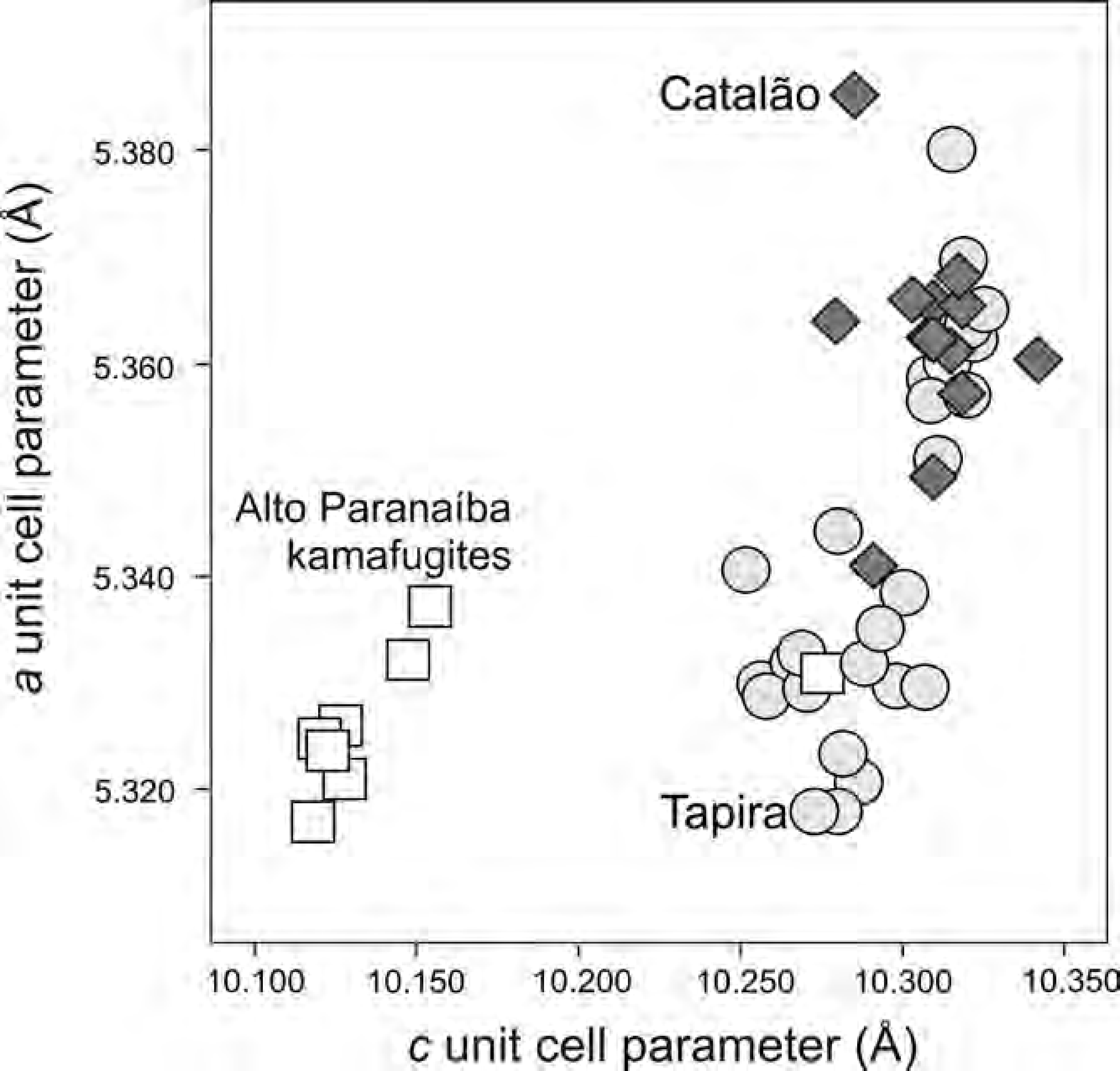
Catalão
Alto Paranaíba
kamafugites
Tapira
5.380
5.360
5.340
5.320
a unit cell parameter (Å)
10.100
10.150
10.200
10.250
10.300
10.350
c unit cell parameter (Å)

(a)

[IV]Al*2

phlogopite

Tapira

Salitre

Araxa

biotite

[VI]Mg

Si/3

Carbonatites

tetraferriphlogopite - tetraferriannite

[IV]Fe*3

X-Ray refinement:

◆ Catalão II

▲ Catalão I

Chemical composition:

◇ Catalão II

△ Catalão I

Alto Paranaiba Igneous Province:

○ Tapira X-Ray refinement

(b)

[IV]Al*2

phlogopite

biotite

[VI]Mg

Si/3

Carbonatites

tetraferriphlogopite - tetraferriannite

[IV]Fe*3

Serra do Mar:

◆ Itatiaia

◇ Jacupiranga

◇ Ipanema

Finland:

✳ Sokli

(c)

[IV]Al*2

Catalão II phlogopite-picrite data:

● X-Ray refinement

□ Chemical composition

phlogopite

biotite

[VI]Mg

Si/3

Carbonatites

tetraferriphlogopite - tetraferriannite

[IV]Fe*3

Alto Paranaiba Igneous Province:

■ Kimberlites

■ Kamafugites

○ Presidente Olegario X-Ray refinement

(d)

[IV]Al*2

phlogopite

biotite

[VI]Mg

Si/3

tetraferriphlogopite - tetraferriannite

[IV]Fe*3

Literature:

● Madagascar

● Jasra

● Sung Valley

● Ischia

○ Central Mediterranean lamproites

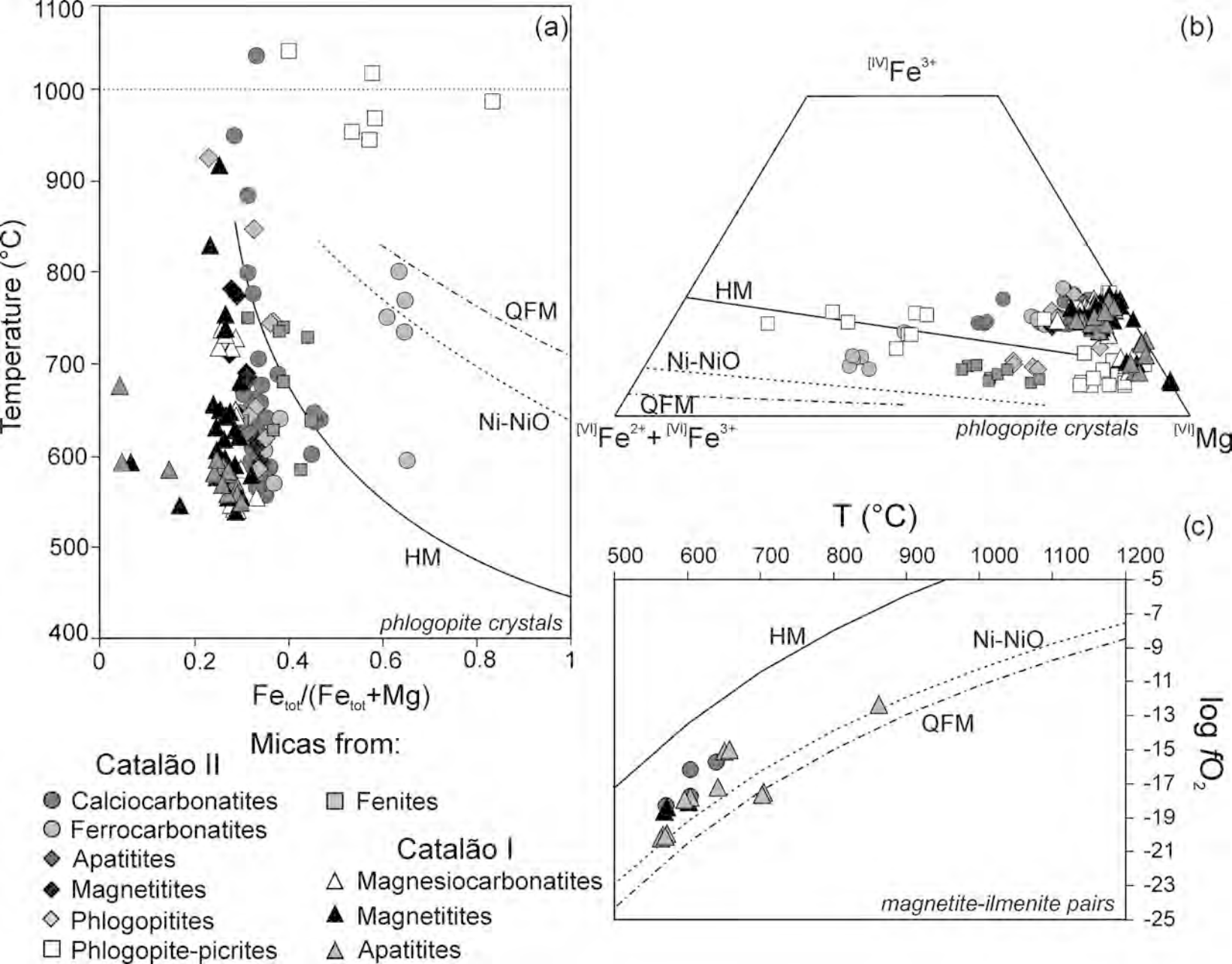
(a)
Temperature (°C)
1100
1000
900
800
700
600
500
400
0
0.2
0.4
0.6
0.8
1
$Fe_{tot}/(Fe_{tot}+Mg)$
QFM
Ni-NiO
HM
phlogopite crystals
(b)
$^{[IV]}Fe^{3+}$
HM
Ni-NiO
QFM
$^{[VI]}Fe^{2+} + {}^{[VI]}Fe^{3+}$
phlogopite crystals
$^{[VI]}Mg$
(c)
T (°C)
500
600
700
800
900
1000
1100
1200
HM
Ni-NiO
QFM
magnetite-ilmenite pairs
log fO_2
-5
-7
-9
-11
-13
-15
-17
-19
-21
-23
-25
Micas from:
Catalão II
Calciocarbonatites
Ferrocarbonatites
Apatitites
Magnetitites
Phlogopitites
Phlogopite-picrites
Fenites
Catalão I
Magnesiocarbonatites
Magnetitites
Apatitites

Table 1. Modal analyses and mica types of the main rocks from the Catalão II and Catalão I complexes.

Site	Rock	Borehole no.	Depth below groundlevel:	Sample	Analyses:			Cb	Phl	Op	Ap	Pcl	Cpx	Am	Afs	Ol	Zrn	Chu	Wadeite	*sum*	*Type of trioctahedral mica*
Catalão II	CaCc	C3B2 (A)	79.2	C2A2	icp-oes	icp-ms	modal analyses	65.7	26.5	4.0	3.8									100	Tetraferriphologopite
Catalão II	Syenite	C3B2 (A)	109.7	C2A6	icp-oes	icp-ms	modal analyses		10.3				29.5	21.2	39.0					100	Fe^{3+}-poor-phlogopite
Catalão II	Phl-Picrite	C3B2 (A)	137.8	C2A8	icp-oes	icp-ms	-														Ti-rich-phlogopite and phlogopite
Catalão II	Phl-Picrite	C3B2 (A)	161.2	C2A10	icp-oes	icp-ms	-														Ti-Fe^{3+}-rich phlogopite
Catalão II	Phlogopitite	C3B2 (A)	165.2	C2A11	icp-oes	icp-ms	modal analyses	2.1	71.5	4.3	22.1									100	Tetraferriphologopite
Catalão II	CaCc	C3B2 (A)	287.0	C2A17	icp-oes	icp-ms	-														Tetraferriphologopite
Catalão II	Phl-Picrite	C3B2 (A)	290.1	C2A18	icp-oes	icp-ms	-														Ti-rich-phlogopite and phlogopite
Catalão II	CaCc	C3B2 (A)	314.0	C2A19	icp-oes	icp-ms	-														Tetraferriphologopite
Catalão II	CaCc	C3B2 (A)	320.0	C2A20	icp-oes	icp-ms	-														Tetraferriphologopite
Catalão II	CaCc	C3B2 (A)	324.8	C2A21	icp-oes	icp-ms	-														Tetraferriphologopite
Catalão II	Magnetitite	C3B2 (A)	353.1	C2A24	icp-oes	icp-ms	modal analyses	7.1	23.1	56.2	6.3	7.3								100	Tetraferriphologopite
Catalão II	Clinopyroxenite	C3B2 (A)	395.7	C2A26	-	-	modal analyses	2.5	24.8		2.0		70.8							100	Fe^{3+}-poor-phlogopite
Catalão II	Apatitite	C3B1 (B)	127.7	C2B3	icp-oes	icp-ms	modal analyses	1.8	43.1	8.2	46.9									100	Tetraferriphologopite
Catalão II	Phlogopitite	C3B1 (B)	158.8	C2B5	-	-	modal analyses	22.9	68.0	0.5	4.2						4.3			100	Fe^{3+}-moderate-phlogopite
Catalão II	FeCc	C3B1 (B)	312.9	C2B18	icp-oes	icp-ms	modal analyses	56.1	26.5	0.1	17.3									100	Tetraferriphologopite
Catalão II	CaCc	C3B1 (B)	328.5	C2B19	icp-oes	icp-ms	-														Tetraferriphologopite
Catalão II	CaCc	C3B1 (B)	354.0	C2B22	icp-oes	icp-ms	-														Tetraferriphologopite
Catalão II	Phl-Picrite	C3B1 (B)	368.8	C2B23	icp-oes	icp-ms	-														Ti-Fe^{3+}-rich phlogopite and phlogopite
Catalão II	FeCc	C3B1 (B)	400.0	C2B24	icp-oes	icp-ms	modal analyses	77.2	17.0	1.8	1.8		1.2						1.0	100	Fe^{3+}-moderate-phlogopite
Catalão I	Magnetitite	F72	88.5	C1A4			modal analyses	5.7	4.6	61.8	20.8	7.1								100	Tetraferriphologopite
Catalão I	Magnetitite	F72	95.0	C1A3			modal analyses	6.0	8.5	56.8	22.2	6.5								100	Tetraferriphologopite
Catalão I	Magnetitite	F72	100.0	C1A5	icp-oes	icp-ms	modal analyses	10.5	12.4	43.6	21.3	4.9				6.5		0.8		100	Tetraferriphologopite
Catalão I	MgCc	3E 19N	99.4	C1B6	-	-	modal analyses	85.3	2.8	7.1	3.1	1.7								100	Tetraferriphologopite
Catalão I	MgCc	49E 33N	121.8	C1C3A	-	-	modal analyses	88.2	2.4	7.6		1.8								100	Tetraferriphologopite
Catalão I	MgCc	49E 33N	121.8	C1C3B	-	-	modal analyses	91.2	1.9	5.4		1.5								100	Tetraferriphologopite
Catalão I	MgCc	49E 33N	130.0	C1C4	icp-oes	icp-ms	-														Tetraferriphologopite
Catalão I	MgCc	49E 33N	143.5	C1C5B	-	-	modal analyses	85.7	2.5	9.0		2.8								100	Tetraferriphologopite
Catalão I	Magnetitite	49E 33N	203.5	C1C8	-	-	modal analyses	6.9	24.4	54.1	6.0	8.6								100	Tetraferriphologopite
Catalão I	Magnetitite	49E 33N	338.3	C1C13	icp-oes	icp-ms	modal analyses	5.8	19.5	66.8	4.5	3.5								100	Tetraferriphologopite
Catalão I	Magnetitite	49E 33N	497.6	C1C20	-	-	modal analyses	15.1	7.5	58.2	11.5	7.7								100	Tetraferriphlogopite and phlogopite
Catalão I	Apatitite	49E 33N	510.0	C1C22	icp-oes	icp-ms	modal analyses	1.6	11.0	22.6	53.6	11.3								100	Tetraferriphlogopite and phlogopite
Catalão I	Magnetitite	49E 33N	520.3	C1C23B	-	-	modal analyses	12.9	15.7	53.6	11.7	6.1								100	Tetraferriphologopite
Catalão I	Apatitite	49E 33N	591.0	C1C26C	-	-	modal analyses	11.5	35.8	7.5	45.2									100	Tetraferriphologopite

Phl-Picrite=Phlogopite-picrite (Guarino et al., 2013); CaCc=Calciocarbonatite; FeCc=Ferrocarbonatite; MgCc=Magnesiocarbonatite; Cb=carbonate mineral; Phl=phlogopite; Op=opaque mineral; Ap=apatite; Pcl=pyrochlore; Cpx=clinopyroxene; Am=amphibole; Afs=alkali-feldspar; Ol=olivine; Zrn=zircone; Chu=clinohumite.

Table 2. Averaged major element analyses (oxide wt%), standard deviations and chemical formulae of mica crystals from representative thin sections of Catalão II and Catalão I. Analyses and chemical formulae of crystals coming from the same thin section but showing remarkable differences in their compositions were not averaged or were averaged over compositionally homogeneous subgroups.

Rock type	Catalão II, Calciocarbonatite														Catalão II, Ferrocarbonatite				Catalão II, Magnetitite		Catalão II, Apatitite	
Sample	C2A2	(s)	C2A17	(s)	C2A19	(s)	C2A20	(s)	C2A21	(s)	C2B19	(s)	C2B22	(s)	C2B18	(s)	C2B24	(s)	C2A24	(s)	C2B3	(s)
N. of crystals	3		4		4		2		9		5		3		3		4		3		3	
chemical composition (oxide wt%)																						
SiO_2	40.98	0.44	41.28	0.88	40.87	0.49	39.93	0.39	41.33	0.90	40.56	0.81	40.03	0.64	39.58	0.85	39.26	0.75	40.50	0.29	40.37	0.55
TiO_2	0.28	0.03	0.23	0.01	0.25	0.02	0.64	0.11	0.34	0.00	0.41	0.11	0.69	0.13	0.47	0.11	1.93	0.21	0.20	0.02	0.30	0.11
Al_2O_3	0.05	0.02	0.03	0.02	0.00	0.02	0.03	0.05	0.23	0.03	0.03	0.01	0.33	0.12	0.08	0.01	5.76	0.82	0.30	0.02	2.12	0.07
Fe_2O_3	17.89	0.98	17.83	0.58	17.69	0.77	23.10	0.86	19.77	0.78	20.88	0.98	19.13	0.98	23.36	0.91	25.06	0.78	17.81	0.71	18.37	1.16
FeO	2.02	0.29	3.79	0.04	3.30	0.00	0.00	0.00	0.00	0.11	0.93	0.29	7.98	0.49	0.00	0.00	3.42	0.14	0.97	0.00	1.64	0.38
MnO	0.12	0.01	0.10	0.01	0.12	0.01	0.05	0.04	0.00	0.01	0.00	0.00	0.85	0.21	0.16	0.04	0.17	0.09	0.14	0.01	0.09	0.01
MgO	24.19	0.92	21.46	0.33	22.77	0.57	21.33	0.98	23.05	0.56	22.28	0.73	17.30	0.96	21.12	0.93	10.23	0.53	25.16	0.57	22.30	0.92
CaO	0.00	0.00	0.41	0.05	0.09	0.01	0.00	0.00	0.11	0.00	0.38	0.12	0.10	0.03	0.15	0.08	0.00	0.00	0.05	0.01	0.00	0.02
BaO	0.05	0.01	0.32	0.04	0.00	0.00	0.00	0.00	0.11	0.05	0.00	0.00	0.00	0.00	0.00	0.00	0.17	0.05	0.00	0.02	0.02	0.01
SrO	0.00	0.00	0.00	0.00	0.00	0.00	0.12	0.04	0.38	0.07	0.10	0.01	0.00	0.00	0.44	0.07	0.37	0.04	0.00	0.00	0.00	0.01
Na_2O	0.14	0.04	0.18	0.02	0.22	0.08	0.18	0.08	0.23	0.02	0.10	0.02	0.03	0.01	0.23	0.05	0.06	0.02	0.10	0.04	0.12	0.03
K_2O	10.26	0.22	10.40	0.31	10.71	0.46	10.65	0.96	10.43	0.21	10.33	0.18	9.67	0.32	10.45	0.58	9.62	0.61	10.17	0.41	10.23	0.26
F	0.00	0.00	0.00	0.00	0.00	0.00	0.00	0.12	0.00	0.11	0.00	0.00	0.00	0.00	0.00	0.00	0.00	0.00	1.17	0.12	0.84	0.15
Sum	95.99		96.03		96.02		96.02		95.98		96.01		96.11		96.04		96.06		96.55		96.39	
chemical formulae (apfu)																						
Si	3.062		3.117		3.079		3.012		3.082		3.045		3.085		2.997		2.986		3.031		3.021	
Al	0.005		0.003		0.000		0.003		0.020		0.003		0.030		0.007		0.516		0.026		0.187	
Fe^{3+}	0.933		0.880		0.921		0.985		0.898		0.952		0.886		0.996		0.497		0.943		0.792	
Sum	4.000		4.000		4.000		4.000		4.000		4.000		4.000		4.000		4.000		4.000		4.000	
Ti	0.016		0.013		0.014		0.036		0.019		0.023		0.040		0.026		0.111		0.011		0.017	
Fe^{2+}	0.126		0.239		0.208		0.000		0.000		0.058		0.514		0.000		0.217		0.060		0.103	
Fe^{3+}	0.073		0.132		0.081		0.326		0.212		0.228		0.224		0.334		0.937		0.060		0.242	
Mn	0.007		0.006		0.008		0.003		0.000		0.000		0.056		0.010		0.011		0.009		0.006	
Mg	2.693		2.415		2.556		2.399		2.562		2.494		1.987		2.384		1.159		2.806		2.487	
Sum	2.916		2.806		2.868		2.764		2.793		2.803		2.820		2.755		2.435		2.947		2.854	
Ca	0.000		0.033		0.007		0.000		0.009		0.031		0.008		0.012		0.000		0.004		0.000	
Ba	0.002		0.009		0.000		0.000		0.003		0.000		0.000		0.000		0.005		0.000		0.001	
Sr	0.000		0.000		0.000		0.005		0.016		0.005		0.000		0.019		0.016		0.000		0.000	
Na	0.020		0.026		0.032		0.026		0.033		0.015		0.005		0.034		0.009		0.014		0.017	
K	0.978		1.001		1.029		1.025		0.992		0.989		0.950		1.009		0.934		0.971		0.976	
Sum	0.999		1.070		1.069		1.056		1.053		1.039		0.963		1.075		0.965		0.989		0.994	
F	0.000		0.000		0.000		0.000		0.000		0.000		0.000		0.000		0.000		0.277		0.198	
$Mg/(Mg+{}^{[VI]}Fe_{tot})$	0.931		0.867		0.898		0.880		0.924		0.897		0.729		0.877		0.501		0.959		0.878	
${}^{[VI]}Ti/{}^{[VI]}Fe^{2+}$	0.13		0.05		0.07		-		-		0.40		0.08		-		0.51		0.19		0.16	
T (K)	923		855		869		-		-		1318		877		-		-		987		962	
T (°C)	649		582		596		-		-		1045		603		-		-		714		689	

Table 2. *continued*

Rock type	Catalão II, Phlogopitite						Catalão II, Phlogopite-picrite								Catalão II, Clinopyroxenite and Syenite				Catalão I, Magnesiocarbonatite			
Sample	C2A11	(s)	C2B5	(s)	C2A8	(s)	C2A10	(s)	C2A18	(s)	C2B23(a)	(s)	C2B23(b)		C2A26	(s)	C2A6	(s)	C1B6	(s)	C1C3A	(s)
N. of crystals	3		3		4		4		6		5		5									
chemical composition (oxide wt%)																						
SiO_2	39.86	0.36	39.67	0.61	39.36	0.64	39.34	0.91	38.05	0.61	40.08	0.84	39.59	0.88	40.58	0.24	40.43	0.35	41.06	0.11	41.21	0.81
TiO_2	0.30	0.02	1.22	0.11	4.02	0.33	2.89	0.28	4.32	0.26	3.55	0.58	4.79	0.26	1.09	0.03	0.95	0.14	0.09	0.02	0.07	0.01
Al_2O_3	0.10	0.05	8.26	0.82	12.32	0.92	2.79	0.92	11.20	0.32	11.15	0.98	1.45	0.91	7.56	1.02	8.85	0.97	0.15	0.06	0.19	0.02
Fe_2O_3	20.12	0.51	7.67	0.58	6.06	0.98	13.71	0.78	10.49	0.78	5.84	0.96	14.01	0.75	9.23	0.98	7.77	0.86	17.66	0.44	17.54	0.58
FeO	2.05	0.28	8.97	0.14	1.41	0.29	14.79	0.14	10.96	0.33	2.85	0.33	0.90	0.14	9.25	0.29	7.35	0.76	0.00	0.00	0.30	0.04
MnO	0.23	0.01	0.24	0.01	0.21	0.05	0.91	0.09	0.18	0.03	0.05	0.02	0.04	0.01	0.63	0.01	0.51	0.04	0.04	0.01	0.08	0.01
MgO	22.83	0.36	19.20	0.58	20.31	0.92	11.71	0.58	9.96	0.53	21.00	0.98	23.45	0.76	16.90	0.92	18.58	0.98	25.51	0.28	25.98	0.38
CaO	0.05	0.01	0.06	0.01	0.00	0.00	0.27	0.00	0.00	0.00	0.14	0.03	0.05	0.01	0.00	0.00	0.18	0.02	0.11	0.07	0.01	0.01
BaO	0.05	0.02	0.11	0.01	0.89	0.11	0.25	0.07	0.32	0.07	0.73	0.11	0.52	0.07	0.00	0.00	0.04	0.03	0.13	0.03	0.02	0.01
SrO	0.00	0.00	0.00	0.01	0.00	0.00	0.00	0.00	0.00	0.00	0.02	0.01	0.17	0.00	0.10	0.02	0.63	0.11	0.16	0.03	0.08	0.01
Na_2O	0.16	0.06	0.04	0.02	0.22	0.04	0.49	0.12	0.45	0.11	0.15	0.04	0.23	0.11	0.22	0.04	0.31	0.08	0.17	0.11	0.14	0.02
K_2O	9.95	0.38	10.04	0.41	9.86	0.52	9.02	0.71	9.66	0.36	10.30	0.72	10.32	0.71	10.14	0.22	10.10	0.98	10.44	0.21	10.25	0.21
F	0.64	0.14	0.95	0.10	2.29	0.00	0.00	0.00	0.82	0.00	0.00	0.00	0.86	0.11	0.55	0.08	0.50	0.12	0.88	0.15	0.22	0.10
Sum	96.34		96.43		96.95		96.17		96.43		95.84		96.38		96.26		96.19		96.40		96.12	
chemical formulae (apfu)																						
Si	3.012		2.963		2.851		3.077		2.884		2.888		2.949		3.041		2.999		3.060		3.054	
Al	0.009		0.727		1.051		0.257		1.001		0.947		0.127		0.668		0.774		0.014		0.017	
Fe^{3+}	0.979		0.311		0.097		0.666		0.116		0.165		0.924		0.291		0.227		0.926		0.929	
Sum	4.000		4.000		4.000		4.000		4.000		4.000		4.000		4.000		4.000		4.000		4.000	
Ti	0.017		0.068		0.219		0.170		0.246		0.192		0.268		0.061		0.053		0.005		0.004	
Fe^{2+}	0.130		0.560		0.086		0.967		0.695		0.171		0.056		0.580		0.456		0.000		0.019	
Fe^{3+}	0.165		0.120		0.233		0.141		0.482		0.151		0.000		0.229		0.206		0.065		0.050	
Mn	0.015		0.015		0.013		0.060		0.012		0.003		0.003		0.040		0.032		0.002		0.005	
Mg	2.572		2.137		2.193		1.365		1.125		2.255		2.604		1.888		2.054		2.834		2.870	
Sum	2.898		2.901		2.743		2.704		2.560		2.773		2.931		2.798		2.801		2.906		2.948	
Ca	0.004		0.005		0.000		0.023		0.000		0.010		0.004		0.000		0.014		0.009		0.001	
Ba	0.002		0.003		0.025		0.008		0.009		0.021		0.015		0.000		0.001		0.004		0.001	
Sr	0.000		0.000		0.000		0.000		0.000		0.001		0.007		0.005		0.027		0.007		0.003	
Na	0.023		0.006		0.031		0.074		0.067		0.021		0.033		0.032		0.045		0.024		0.020	
K	0.959		0.957		0.911		0.900		0.934		0.947		0.981		0.969		0.956		0.993		0.969	
Sum	0.988		0.971		0.967		1.005		1.010		1.000		1.040		1.005		1.044		1.036		0.994	
F	0.154		0.224		0.525		0.000		0.195		0.000		0.203		0.130		0.116		0.000		0.000	
$Mg/(Mg+{}^{[VI]}Fe_{tot})$	0.897		0.758		0.873		0.552		0.489		0.875		0.979		0.700		0.756		0.978		0.977	
${}^{[VI]}Ti/{}^{[VI]}Fe^{2+}$	0.13		0.12		2.56		0.18		0.35		1.12		4.79		0.11		0.12		-		0.21	
T (K)	929		919		-		977		1234		-		-		903		913		-		1015	
T (°C)	656		646		-		703		961		-				630		640		-		742	

Table 2. *continued*

Rock type	Catalão I, Magnesiocarbonatite												Catalão I, Magnetitite									
Sample	C1C3B	(s)	C1C4	(s)	C1C5B	(s)	C1A3	(s)	C1A4	(s)	C1A5	(s)	C1C8	(s)	C1C13	(s)	C1C20 (a)	(s)	C1C20 (b)	(s)	C1C23B	(s)
N. of crystals	7		3		8		4		3		8		7		3		2		2		4	
	chemical composition (oxide wt%)																					
SiO_2	41.14	0.90	41.52	0.55	41.01	0.88	40.99	0.60	41.87	0.58	41.06	0.41	40.21	0.68	41.40	0.11	40.96	0.23	41.20	0.31	40.93	0.49
TiO_2	0.00	0.00	0.37	0.09	0.00	0.00	0.08	0.10	0.09	0.11	0.11	0.08	0.00	0.02	0.09	0.01	0.06	0.02	0.07	0.02	0.21	0.13
Al_2O_3	0.19	0.03	1.23	0.05	3.95	0.25	0.13	0.12	0.03	0.07	0.04	0.09	0.00	0.02	0.01	0.01	0.04	0.03	10.96	0.14	0.30	0.47
Fe_2O_3	16.60	0.78	15.74	0.58	10.21	0.98	17.20	0.76	15.23	1.36	17.22	1.12	18.98	0.72	17.72	0.08	15.49	0.81	2.74	0.48	16.97	1.36
FeO	2.30	0.11	0.35	0.12	3.48	0.69	0.20	0.31	0.60	0.34	0.11	0.41	0.00	0.00	0.00	0.00	2.43	0.28	0.98	0.63	0.84	0.11
MnO	0.02	0.01	0.11	0.01	0.17	0.03	0.02	0.03	0.01	0.01	0.08	0.06	0.23	0.00	0.02	0.00	0.07	0.02	0.04	0.01	0.03	0.03
MgO	24.36	0.56	24.90	0.47	25.34	0.71	25.91	0.53	26.84	0.72	26.83	0.55	25.88	0.61	26.33	0.10	25.93	0.42	27.28	0.09	24.86	0.48
CaO	0.00	0.00	0.04	0.02	0.07	0.01	0.11	0.07	0.05	0.06	0.00	0.00	0.10	0.16	0.01	0.01	0.03	0.01	0.00	0.00	0.04	0.07
BaO	0.15	0.05	0.00	0.00	0.05	0.02	0.06	0.07	0.01	0.01	0.01	0.01	0.08	0.01	0.00	0.00	0.02	0.01	0.27	0.05	0.15	0.21
SrO	0.27	0.07	0.66	0.02	0.01	0.01	0.39	0.13	0.16	0.14	0.01	0.01	0.16	0.02	0.00	0.02	0.00	0.00	0.00	0.00	0.18	0.20
Na_2O	0.18	0.02	0.16	0.04	0.03	0.02	0.10	0.11	0.07	0.04	0.10	0.02	0.27	0.09	0.06	0.02	0.15	0.03	0.05	0.02	0.25	0.11
K_2O	10.47	0.21	10.86	0.31	10.96	0.18	10.78	0.31	10.99	0.20	10.39	0.34	10.07	0.21	10.30	0.11	10.23	0.18	10.87	0.17	10.81	0.18
F	1.02	0.11	0.00	0.00	1.25	0.43	0.00	0.00	0.00	0.00	0.00	0.00	0.00	0.00	0.00	0.00	1.12	0.22	2.56	0.22	0.00	0.00
Sum	96.71		95.94		96.53		95.97		95.95		95.96		95.98		95.94		96.53		97.02		95.57	
	chemical formulae (apfu)																					
Si	3.100		3.075		3.039		3.050		3.094		3.038		2.998		3.060		3.065		2.951		3.063	
Al	0.017		0.107		0.344		0.011		0.002		0.004		0.000		0.001		0.003		0.925		0.027	
Fe^{3+}	0.883		0.818		0.617		0.939		0.904		0.958		1.002		0.940		0.932		0.124		0.910	
Sum	4.000		4.000		4.000		4.000		4.000		4.000		4.000		4.000		4.000		4.000		4.000	
Ti	0.000		0.020		0.000		0.004		0.005		0.006		0.000		0.005		0.003		0.004		0.012	
Fe^{2+}	0.145		0.022		0.215		0.012		0.037		0.007		0.000		0.000		0.152		0.059		0.053	
Fe^{3+}	0.058		0.059		0.000		0.024		0.000		0.001		0.063		0.046		0.000		0.023		0.045	
Mn	0.002		0.007		0.010		0.002		0.000		0.005		0.014		0.001		0.004		0.002		0.002	
Mg	2.736		2.748		2.798		2.873		2.956		2.960		2.876		2.900		2.892		2.912		2.773	
Sum	2.940		2.857		3.023		2.915		2.998		2.978		2.953		2.952		3.052		3.000		2.884	
Ca	0.000		0.003		0.005		0.008		0.004		0.000		0.008		0.001		0.002		0.000		0.003	
Ba	0.004		0.000		0.001		0.001		0.000		0.000		0.002		0.000		0.000		0.007		0.004	
Sr	0.011		0.028		0.000		0.016		0.006		0.000		0.007		0.000		0.000		0.000		0.008	
Na	0.026		0.023		0.004		0.013		0.010		0.015		0.039		0.008		0.022		0.007		0.036	
K	1.000		1.025		1.035		1.022		1.036		0.981		0.958		0.971		0.977		0.993		1.032	
Sum	1.041		1.079		1.045		1.060		1.056		0.996		1.014		0.980		1.001		1.007		1.084	
F	0.000		0.000		0.000		0.000		0.000		0.000		0.000		0.000		0.264		0.580		0.000	
$Mg/(Mg+{}^{[VI]}Fe_{tot})$	0.931		0.972		0.929		0.988		0.988		0.998		0.979		0.984		0.950		0.973		0.966	
${}^{[VI]}Ti/{}^{[VI]}Fe^{2+}$	0.00		0.94		-		0.33		0.13		0.91		-		-		0.02		0.07		0.22	
T (K)	-		-		-		1197		932		-		-		-		829		868		1032	
T (°C)	-		-		-		923		658		-		-		-		556		594		758	

Table 2. *continued*

Rock type	Catalão I, Apatitite							
Sample	C1C22 (a)	(s)	C1C22 (b)	(s)	C1C26 (a)	(s)	C1C26 (b)	(s)
N. of crystals	4		4		3		6	
	chemical composition (oxide wt%)							
SiO_2	41.42	0.19	40.65	0.22	41.58	0.18	41.21	0.36
TiO_2	0.09	0.02	0.04	0.02	0.10	0.01	0.48	0.02
Al_2O_3	0.03	0.02	12.55	1.12	0.62	0.10	6.94	0.55
Fe_2O_3	18.30	0.81	2.22	0.85	15.81	0.31	8.47	0.51
FeO	0.00	0.00	0.23	0.00	1.22	0.02	0.46	0.08
MnO	0.02	0.01	0.00	0.00	0.05	0.01	0.07	0.01
MgO	25.59	0.55	27.85	0.61	26.23	0.18	26.90	0.16
CaO	0.03	0.01	0.02	0.01	0.00	0.00	0.01	0.01
BaO	0.06	0.02	1.82	0.18	0.00	0.00	0.12	0.02
SrO	0.00	0.00	0.00	0.00	0.00	0.00	0.00	0.00
Na_2O	0.14	0.06	0.11	0.06	0.06	0.01	0.04	0.06
K_2O	10.26	0.30	10.27	0.42	10.28	0.22	10.57	0.30
F	0.00	0.00	0.00	0.00	0.00	0.00	1.09	0.04
Sum	95.95		95.77		95.94		96.36	
	chemical formulae (apfu)							
Si	3.066		2.882		3.070		2.976	
Al	0.003		1.049		0.054		0.591	
Fe^{3+}	0.931		0.069		0.877		0.434	
Sum	4.000		4.000		4.000		4.000	
Ti	0.005		0.002		0.005		0.026	
Fe^{2+}	0.000		0.013		0.075		0.028	
Fe^{3+}	0.089		0.049		0.001		0.026	
Mn	0.001		0.000		0.003		0.004	
Mg	2.824		2.943		2.886		2.894	
Sum	2.914		3.007		2.971		2.979	
Ca	0.003		0.001		0.000		0.001	
Ba	0.002		0.050		0.000		0.003	
Sr								
Na	0.020		0.015		0.008		0.006	
K	0.969		0.929		0.968		0.974	
Sum	0.994		0.996		0.977		0.984	
F	0.000		0.000		0.000		0.249	
$Mg/(Mg+{}^{[VI]}Fe_{tot})$	0.970		0.979		0.974		0.982	
${}^{[VI]}Ti/{}^{[VI]}Fe^{2+}$	-		0.15		0.07		0.94	
T (K)	-		952		871		-	
T (°C)	-		679		597		-	

Table 3. Major element analyses (oxide wt%) and chemical formulae of mica crystals from Catalão II and Catalão I complexes used in single-crystal X-ray diffraction study.

	Catalão II complex									Catalão I complex				
Rock type	Calciocarbonatite				Ferro-carbonatite	Magnetitite	Phlogopitite	Phlogopite-picrite	Clinopyroxenite	Magnesio-carbonatite	Magnetitite			Apatitite
Sample	C2A2	C2A20	C2A21	C2B19	C2B24	C2A24	C2A11	C2B23	C2A26	C1C4	C1A5	C1C13	C1C20	C1C22
chemical composition (oxide wt%)														
SiO_2	42.22	41.11	41.30	41.55	37.63	41.99	41.09	39.20	39.14	42.10	42.13	41.80	42.93	42.87
TiO_2	0.27	0.76	0.54	0.65	1.92	0.74	0.61	4.70	1.04	0.11	0.31	0.09	0.03	0.10
Al_2O_3	0.06	0.00	0.00	0.03	6.23	0.31	0.69	2.40	7.31	0.43	0.00	0.00	6.03	0.26
FeO	4.08	4.28	4.84	4.07	24.74	2.71	5.20	0.68	15.92	1.89	5.59	3.10	2.88	2.47
Fe_2O_3	15.42	16.07	15.80	15.71	6.61	15.38	14.97	15.85	5.88	15.15	14.85	15.85	7.05	14.57
MnO	0.10	0.34	0.12	0.14	0.18	0.13	0.11	0.04	0.51	0.08	0.15	0.06	0.04	0.04
MgO	23.17	22.94	22.91	23.23	9.18	23.99	22.61	22.59	15.97	25.39	22.39	24.65	25.30	24.99
CaO	0.00	0.00	0.00	0.00	0.00	0.00	0.00	0.05	0.01	0.00	0.00	0.00	0.03	0.00
SrO	0.00	0.10	0.14	0.10	0.00	0.00	0.00	0.26	0.09	0.05	0.05	0.05	0.10	0.00
Na_2O	0.21	0.18	0.32	0.15	0.28	0.21	0.14	0.23	0.12	0.18	0.38	0.16	0.19	0.14
K_2O	10.23	10.10	9.83	10.21	9.37	10.26	10.18	9.92	9.99	10.33	10.07	10.19	10.82	10.39
Cr_2O_3	0.06	0.00	0.00	0.00	0.00	0.00	0.00	0.00	0.00	0.00	0.00	0.00	0.00	0.00
F	0.45	1.41	1.57	1.16	0.50	1.22	1.01	0.84	0.66	0.66	0.20	0.25	2.38	0.75
H_2O	3.80	3.30	3.25	3.45	3.50	3.45	3.50	3.54	3.60	3.70	3.90	3.90	3.02	3.70
O = F	-0.19	-0.59	-0.66	-0.49	-0.21	-0.51	-0.42	-0.35	-0.28	-0.27	-0.08	-0.11	-1.00	-0.32
Sum	99.88	100.00	99.96	99.96	99.93	99.88	99.69	99.95	99.96	99.80	99.94	99.99	99.80	99.96
Unit-cell content recalculated on the basis of $O_{12-(x+y)}(OH)_xF_y$														
$^{[IV]}Si$	3.155	3.093	3.107	3.115	3.013	3.123	3.096	2.908	3.000	3.121	3.164	3.114	3.109	3.167
$^{[IV]}Al$	0.005	0.000	0.000	0.003	0.588	0.027	0.061	0.210	0.660	0.038	0.000	0.000	0.515	0.023
$^{[IV]}Fe^{3+}$	0.840	0.907	0.893	0.882	0.399	0.850	0.843	0.882	0.340	0.841	0.836	0.886	0.376	0.810
$^{[IV]}Sum$	4.000	4.000	4.000	4.000	4.000	4.000	4.000	4.000	4.000	4.000	4.000	4.000	4.000	4.000
$^{[VI]}Mg$	2.581	2.573	2.569	2.596	1.096	2.660	2.539	2.498	1.825	2.805	2.506	2.737	2.731	2.752
$^{[VI]}Fe^{3+}$	0.027	0.003	0.001	0.004	0.000	0.011	0.006	0.002	0.000	0.004	0.003	0.002	0.008	0.000
$^{[VI]}Fe^{2+}$	0.255	0.269	0.304	0.255	1.657	0.169	0.328	0.042	1.021	0.117	0.351	0.193	0.174	0.153
$^{[VI]}Cr^{3+}$	0.004	0.000	0.000	0.000	0.000	0.000	0.000	0.000	0.000	0.000	0.000	0.000	0.000	0.000
$^{[VI]}Mn^{2+}$	0.006	0.022	0.008	0.009	0.012	0.008	0.007	0.003	0.033	0.005	0.010	0.004	0.002	0.003
$^{[VI]}Ti^{4+}$	0.015	0.043	0.031	0.037	0.116	0.041	0.035	0.262	0.060	0.006	0.018	0.005	0.002	0.006
$^{[VI]}Sum$	2.888	2.910	2.913	2.901	2.881	2.889	2.915	2.807	2.939	2.937	2.888	2.941	2.918	2.914
$^{[XII]}Ca$	0.000	0.000	0.000	0.000	0.000	0.000	0.000	0.004	0.001	0.000	0.000	0.000	0.002	0.000
$^{[XII]}Na$	0.030	0.026	0.047	0.022	0.043	0.030	0.020	0.033	0.018	0.026	0.055	0.023	0.026	0.020
$^{[XII]}K$	0.975	0.969	0.943	0.976	0.957	0.973	0.978	0.939	0.977	0.977	0.965	0.968	0.999	0.979
$^{[XII]}Sr$	0.000	0.004	0.006	0.004	0.000	0.000	0.000	0.011	0.004	0.002	0.002	0.002	0.004	0.000
$^{[XII]}Sum$	1.005	0.999	0.996	1.002	1.000	1.003	0.998	0.987	1.000	1.005	1.022	0.993	1.031	0.999
F	0.106	0.336	0.372	0.275	0.127	0.287	0.241	0.197	0.160	0.155	0.047	0.059	0.543	0.175
OH	1.894	1.656	1.629	1.725	1.869	1.712	1.759	1.752	1.840	1.829	1.953	1.938	1.457	1.823
O	10.000	10.008	10.000	10.000	10.004	10.001	10.000	10.051	10.000	10.016	10.000	10.003	10.000	10.002
Octahedral sites mean electron count														
$M1_{Xref}$	12.89(6)	13.37(6)	13.42(5)	12.89(6)	20.15(8)	12.41(5)	13.28(8)	12.29(8)	17.28(6)	12.32(5)	13.50(8)	12.45(5)	12.67(8)	12.41(7)
$M2_{Xref}$	12.62(6)	13.22(5)	13.21(4)	12.72(5)	19.75(7)	12.31(4)	13.26(7)	12.16(6)	16.78(6)	12.27(4)	13.33(7)	12.35(4)	12.58(7)	12.31(6)
$M1+2M2_{(Xref)}$	38.1	39.8	39.8	38.3	59.7	37.0	39.8	36.6	50.8	36.9	40.2	37.2	37.8	37.0
$M1+2M2_{Epma}$	38.9	39.4	39.6	38.9	59.1	37.7	40.1	37.0	50.6	37.1	39.9	38.1	37.6	37.2
Interlayer site mean electron count														
A_{Xref}	18.3(2)	18.6(2)	19	18.0(2)	18.6(3)	18.3(2)	18.4(2)	18.1(2)	18.1(2)	18.7(2)	18.3(2)	18.2(2)	18.6(2)	18.0(2)
A_{Epma}	18.9	18.8	18.6	18.9	18.7	18.8	18.8	18.6	18.9	18.9	19.0	18.7	19.4	18.8
$^{[VI]}Ti/^{[VI]}Fe^{2+}$	0.06	0.16	0.10	0.15	0.07	0.24	0.11	6.24	0.06	0.05	0.05	0.03	0.01	0.04
T (K)	860	959	899	943	870	1059	904		860	853	853	832	820	843
T (°C)	586	686	626	670	596	786	631		586	580	580	558	547	569

Note: Xref = single crystal X-ray refinement; Epma = electron probe microanalysis

Table 4. Relevant cation-anion bond lengths of refined Catalão II and Catalão I *M* micas.

	Catalão II									Catalão I				
Rock Type	Calciocarbonatite				Ferro-carbonatite	Magnetitite	Phlogopitite	Phlogopite-picrite	Clinopyroxenite	Magnesio-carbonatite	Magnetitite			Apatitite
Sample	C2A2	C2A20	C2A21	C2B19	C2B24	C2A24	C2A11	C2B23	C2A26	C1C4	C1A5	C1C13	C1C20	C1C22
Tetrahedron														
T-O1	1.681(1)	1.678(1)	1.678(1)	1.676(1)	1.666(2)	1.680(1)	1.680(2)	1.679(2)	1.664(1)	1.667(1)	1.680(1)	1.677(1)	1.676(2)	1.679(1)
T-O1'	1.681(1)	1.680(1)	1.678(1)	1.679(1)	1.668(2)	1.678(1)	1.680(2)	1.678(2)	1.664(1)	1.667(1)	1.676(2)	1.678(1)	1.680(2)	1.680(1)
T-O2	1.6792(7)	1.6756(8)	1.6767(7)	1.6775(6)	1.6628(9)	1.6790(6)	1.6797(8)	1.6767(9)	1.6621(6)	1.6665(6)	1.6790(8)	1.6766(5)	1.6765(8)	1.6777(7)
T-O3	1.676(1)	1.679(1)	1.675(1)	1.6778(8)	1.676(2)	1.6788(8)	1.681(1)	1.676(1)	1.666(1)	1.6657(9)	1.678(1)	1.6782(6)	1.674(1)	1.677(1)
⟨T-O⟩	1.679	1.678	1.677	1.678	1.668	1.679	1.680	1.677	1.664	1.667	1.678	1.677	1.677	1.678
Tetrahedral Parameters														
α (°)	11.25	11.18	10.72	10.83	5.98	11.33	11.15	11.32	6.33	9.55	11.13	11.12	11.12	11.18
τ (°)	109.96	109.98	109.95	109.90	110.23	109.93	109.99	109.84	110.47	110.26	110.02	110.04	110.07	109.99
Δz (Å)	0.005	0.006	0.003	0.002	0.007	0.002	0.007	0.006	0.007	0.003	0.003	0.007	0.007	0.005
Tetrahedral tickness	2.276	2.278	2.275	2.276	2.270	2.278	2.280	2.275	2.268	2.271	2.280	2.275	2.277	2.278
<O-O>basal (Å)	2.430	2.424	2.420	2.423	2.380	2.428	2.434	2.429	2.363	2.375	2.424	2.422	2.420	2.427
Tetrahedral volume (Å^3)	2.735	2.731	2.731	2.732	2.707	2.734	2.735	2.737	2.699	2.709	2.731	2.732	2.730	2.733
Octahedron (M1)														
M1-O3 (×4)	2.1040(9)	2.0999(9)	2.1034(9)	2.1031(7)	2.110(1)	2.1007(7)	2.106(1)	2.105(1)	2.1095(9)	2.0962(8)	2.102(1)	2.1006(6)	2.103(1)	2.1013(9)
M1-O4 (×2)	2.060(1)	2.057(1)	2.059(1)	2.058(1)	2.088(2)	2.055(1)	2.064(1)	2.058(1)	2.075(1)	2.050(1)	2.050(1)	2.055(1)	2.054(2)	2.057(1)
⟨M1-O⟩	2.089	2.086	2.089	2.088	2.103	2.085	2.092	2.089	2.098	2.081	2.085	2.085	2.087	2.087
Octahedron (M2)														
M2-O3' (×2)	2.103(1)	2.100(1)	2.1030(1)	2.0961(7)	2.111(2)	2.1005(8)	2.102(1)	2.105(2)	2.1072(9)	2.0949(9)	2.095(1)	2.1018(6)	2.103(1)	2.100(1)
M2-O3 (×2)	2.0962(9)	2.094(1)	2.096(1)	2.1022(8)	2.108(1)	2.0927(8)	2.098(1)	2.096(1)	2.099(1)	2.0869(8)	2.096(1)	2.0925(6)	2.090(1)	2.092(1)
M2-O4 (×2)	2.0671(9)	2.064(1)	2.064(1)	2.065(1)	2.070(1)	2.063(1)	2.067(1)	2.066(1)	2.0615(9)	2.059(1)	2.065(1)	2.063(1)	2.064(1)	2.064(1)
⟨M2-O⟩	2.089	2.086	2.088	2.081	2.096	2.085	2.089	2.089	2.089	2.080	2.085	2.086	2.086	2.085
Octahedral parameters														
⟨O3-O3⟩	3.098	3.093	3.098	3.099	3.108	3.095	3.098	3.098	3.097	3.084	3.094	3.096	3.093	3.095
Octahedral tickness	2.157	2.155	2.153	2.153	2.176	2.149	2.162	2.157	2.172	2.151	2.149	2.154	2.156	2.149
Interlayer cation														
A-O1 (×4)	2.935(1)	2.932(1)	2.946(1)	2.946(1)	3.048(2)	2.933(1)	2.942(2)	2.942(2)	3.036(1)	2.963(1)	2.936(1)	2.934(1)	2.938(2)	2.934(1)
A-O2 (× 2)	2.940(2)	2.938(2)	2.947(2)	2.944(2)	3.055(2)	2.932(8)	2.942(2)	2.945(2)	3.033(2)	2.962(2)	2.927(2)	2.935(1)	2.941(2)	2.938(2)
A-O1' (×4)	3.454(1)	3.448(2)	3.439(1)	3.442(1)	3.325(2)	3.452(1)	3.454(2)	3.447(1)	3.323(1)	3.397(1)	3.444(2)	3.454(1)	3.441(2)	3.448(2)
A-O2' (× 2)	3.454(1)	3.447(2)	3.439(2)	3.445(2)	3.328(3)	3.456(2)	3.454(2)	3.451(2)	3.333(2)	3.401(2)	3.445(2)	3.457(2)	3.446(2)	3.451(2)
$\langle A\text{-}O\rangle_{inner}$	2.937	2.934	2.946	2.945	3.050	2.933	2.942	2.943	3.035	2.963	2.933	2.934	2.939	2.935
$\langle A\text{-}O\rangle_{outer}$	3.454	3.448	3.439	3.443	3.326	3.453	3.454	3.448	3.326	3.398	3.444	3.455	3.443	3.449
A-O4	4.056	4.057(1)	4.053(1)	4.056(1)	4.015(2)	4.061(1)	4.064(1)	4.059(2)	4.016(3)	4.049(1)	4.056(1)	4.055(1)	4.059	4.056(1)
Interlayer separation	3.455	3.451	3.444	3.450	3.412	3.453	3.464	3.455	3.414	3.442	3.441	3.449	3.452	3.450

Table 5. The $^{[IV]}Fe^{3+}$ variation in phlogopite crystals related to their drill-core depth in the Catalão II and Catalão I rocks.

Catalão II complex

Borehole C3B2(A)	Phlogopite-picrites			Calciocarbonatites					Magnetitite	Phlogopitite	Fenites	
	C2A8	C2A10	C2A18	C2A2	C2A17	C2A19	C2A20	C2A21	C2A24	C2A11	C2A6	C2A26
$^{[IV]}Fe^{3+}$	0.097	0.666	0.116	0.933	0.880	0.921	0.985	0.898	0.943	0.979	0.227	0.291
Depth	-137.8	-161.2	-290.1	-79.2	-287.0	-314.0	-320.0	-324.8	-353.1	-165.2	-109.7	-395.7

Borehole C3B1(B)	Apatitite	Phlogopitite	Calciocarbonatites		Phlogopite-picrite		Ferrocarbonatites	
	C2B3	C2B5	C2B19	C2B22	C2B23(a)	C2B23(b)	C2B18	C2B24
$^{[IV]}Fe^{3+}$	0.792	0.311	0.952	0.886	0.165	0.924	0.996	0.497
Depth	-127.7	-158.8	-328.5	-354.0	-368.8	-368.8	-312.9	-400.0

Catalão I complex

Borehole F72	Magnetitites		
	C1A4	C1A3	C1A5
$^{[IV]}Fe^{3+}$	0.939	0.904	0.958
Depth	-88.5	-95.0	-100.0

Borehole 3E19N Magnesiocarbonatite	
	C1B6
$^{IV}Fe^{3+}$	0.926
Depth	-99.4

Borehole 49E33N	Magnesiocarbonatites				Magnetitites					Apatitites			
	C1C3A	C1C3B	C1C4	C1C5B	C1C8	C1C13	C1C20 (a)	C1C20 (b)	C1C23B	C1C26 (a)	C1C26 (b)	C1C22 (a)	C1C22 (b)
$^{[IV]}Fe^{3+}$	0.929	0.883	0.818	0.617	1.002	0.940	0.932	0.124	0.910	0.877	0.434	0.931	0.069
Depth	-121.8	-121.8	-130.0	-143.5	-203.5	-338.3	-497.6	-497.6	-520.3	-591.0	-591.0	-510.0	-510.0

Note: $^{[IV]}Fe^{3+}$ values are taken from Table 2.

Table 6. Range of temperature estimated on phlogopite crystals for Catalão II and Catalão I rocks, and those obtained for few Catalão magnetite-ilmenite pairs.

	Rock	T (°C) *phlogopite crystals*	T (°C) *magnetite-ilmenite pairs*
Catalão II complex	Calciocarbonatites	1045-890 °C 804-558 °C	640-571 °C
	Ferrocarbonatites	806-571 °C	
	Magnetitites	786-647 °C	
	Apatitites	689-594 °C	
	Phlogopitites	932-587 °C	
	Phlogopite-picrites	1050-952 °C 703-631 °C	
	Fenites	754-586 °C	
Catalão I complex	Magnesiocarbonatites	742-542 °C	
	Magnetitites	923-540 °C	605-568 °C
	Apatitites	679-550 °C	862-564 °C